行政院國家科學委員會專題研究計畫　成果報告

大白鼠三叉神經運動核背後側之中間神經元特性及其與運動神經元間的突觸傳導特性之研究(2/2)

計畫類別：個別型計畫
計畫編號：NSC91-2320-B-039-007-
執行期間：91 年 08 月 01 日至 92 年 07 月 31 日
執行單位：中國醫藥大學生理學科

計畫主持人：閔明源

報告類型：完整報告

處理方式：本計畫涉及專利或其他智慧財產權，2 年後可公開查詢

中　華　民　國 92 年 10 月 23 日

（二）中英文摘要與關鍵辭

關鍵辭：節律性咀嚼運動、膜生理特性、運動神經元、中間神經元、三叉神經

中文摘要

在本計畫中，我們分析了位於三叉神經運動核後側與顏面神經運動核前沿間之中間神經元的形態與生理特性。過去的研究顯示：位於此區域之許多中間神經細胞可能參與產生節率性咀嚼運動的神經控制。我們使用取自 5-8 天大的新生大鼠的腦幹縱切薄片為實驗材料。在以近紅外線照明之微分干擾相位差顯微鏡配合適當的影像系統的輔助下，位於三叉神經運動核後側之中間神經元可在新鮮的腦幹薄片中被觀察鑑定，之後我們使用填充以 K-gluconate 與 biocytin 為主的玻璃電極對被觀察鑑定之中間神經元作全胞型之胞內紀錄。本計畫共紀錄了 127 個中間神經元，以他們對應於由電極注射去極化電流之放射動作電位形式為基礎，我們將這些細胞歸類為三個主要的類型，亦既連續型放射（類型一）、爆衝型放射（類型二）與適應型放射（類型三）。與類型二細胞比較，類型一細胞有較大的「輸入阻抗」因此對應有較低的被興奮閾值。在所有三種類型的細胞中，當以方形的過極化電流波注射細胞時，其對應的細胞膜電位變化過程中均有「sag」產生；此外，對應於去極化電流的注射，膜電位的改變有「rectification」的特性，尤其以類型二細胞較類型一細胞明顯。我們總共對 63 個細胞注射以 biocytin 以供生理特性紀錄後對細胞形態研究；其中有 44 個細胞其軸突與其分支可被清楚鑑定出。我們發現所有類型細胞中，都有例子可以看到他們的軸突分枝延伸入腦幹幾個相關區域，包括「小細胞網狀核區」、「三叉神經運動核」、「上三叉神經核」或「三叉神經中腦核」等區域。在 44 個中的 25 個細胞，其軸突投射區域可達兩個以上目標，包含三叉神經運動核與述區域中的一或數個。當以高（100x）倍物鏡觀察時，可發現許多細胞的軸突有分枝出 varicosities 與終末梢，在三叉神經運動核中這些 varicosities 與終末梢被發現鄰近於此區域內之細胞的本體上，此外他們也可以被發現鄰近於被紀錄細胞附近之其他中間神經元的細胞本體上。這些結果顯示，中間神經元可能與三叉神經運動神經元及鄰近的其他中間神經元形成突觸連結。以上結果提供有關三叉神經運動核週邊之中間神經元的膜生理特性資訊與這些細胞與鄰近之其他中間神經元及三叉神經運動神經元間有突觸連結的證據。因此可以推論位於三叉神經運動核後側與顏面神經運動核前沿間之中間神經元可能會修飾甚至參與產生節率性咀嚼運動指令到運動神經元。

本計畫成果結合部分中山醫學大學楊琇雯博士（助理教授）計畫成果（*NSC 91-2320-B-040-021*）已被接受在 European Journal of Neuroscience 發表。部分成果也將成為參與本計畫之研究生的碩士論文（許珮倩，中國醫藥大學醫學研究所）。所附為被接受論文之完整稿件。

（二）英文摘要與關鍵辭

Keywords：Rhythmical Jaw Movement、Membrane Physiology、Motoneuron、Interneuron、Trigeminal

In this study, we have characterized the membrane properties and morphology of interneurones that lie between the caudal pole of the trigeminal motor nucleus and the rostral border of the facial motor nucleus. Previous studies suggest that many of these interneurones may participate in the genesis of rhythmical jaw movements. Saggital brainstem slices were taken from rats aged 5-8 days. Interneurones lying caudal to the trigeminal motor nucleus were visualized using near infrared differential interference contrast (DIC) microscopy, and were recorded from using patch pipettes filled with a K-gluconate and biocytin based solution. The 127 neurones recorded could be categorized into three subtypes on the basis of their responses to injection of depolarising current pulses; namely tonic firing (type I), burst firing (type II) and spike-adaptive (type III) neurones. Type I interneurones had a higher input resistance, and a lower rheobase than type II neurones. All three neurone subtypes showed “sag” of the voltage response to injection of large amplitude hyperpolarizing current pulses, and, in addition, also showed rectification of the voltage response to injection of depolarising current pulses, with type II neurones showing significantly greater rectification than type I neurones. The axonal arborisations were reconstructed for 44 of 63 neurones labelled with tracer. Neurons of each subtype were found to issue axon collaterals terminating in the brainstem nuclei, including the parvocellular reticular nucleus (PCRt), the trigeminal motor nucleus (Vmot), the supratrigeminal nucleus or the trigeminal mesencephalic nucleus. Twenty-five of the 43 neurones issued collaterals that terminate in the Vmot and the other brainstem nuclei. When viewed under 100x magnification, the collaterals of some interneurones were seen to give off varicosities and end-terminations that passed close to the somata of unidentified neurones in the trigeminal motor nucleus and in the area close to the interneurone soma itself. This suggests that the interneurones may make synaptic contacts on both motoneurones and also on nearby interneurones. These results provide data on the membrane properties of trigeminal interneurones and evidence for their synaptic connections with both nearby interneurones and also with motoneurones. Thus, the interneurones examined could play roles both in the shaping, and possibly also in the generation, of rhythmical signals to trigeminal motoneurones.

The results of this project together with part of results of other project (*NSC 91-2320-B-040-021,* Dr. Yang’s (Department of Life Sciences at Chung Shan Medical University) have been accepted for publication in European Journal of Neuroscience.

Some of the results also form the Master Thesis of Miss Hsu (Institute of Medicine, China Medical University). The accepted manuscript is attached.

The Physiological and Morphological Characteristics of Interneurones Caudal to the Trigeminal Motor Nucleus in Rats

[1]Ming-Yuan Min, [1,2]Pei-Chien Hsu, [2]Hsiu-Wen Yang

[1]Department of Physiology, China Medical University, Taichung 404,
[2]Department of Life Sciences, Chung Shan Medical University, Taichung 402,
Taiwan.

Correspondence should be addressed to:
Drs. Hsiu-Wen Yang & Ming-Yuan Min as above.

Running Title: Properties of Interneurones Caudal to the Vmot

Key words: rhythmical jaw movements; membrane properties; motoneurones.

Number of pages: 51, including this page, 2 tables and 10 figures. The whole manuscript 8838 words, Abstract 260 words, Introduction 406 words.

Abstract

In this study, we have characterized the membrane properties and morphology of interneurones that lie between the caudal pole of the trigeminal motor nucleus and the rostral border of the facial motor nucleus. Previous studies suggest that many of these interneurones may participate in the genesis of rhythmical jaw movements. Saggital brainstem slices were taken from rats aged 5-8 days. Interneurones lying caudal to the trigeminal motor nucleus were visualized using near infrared differential interference contrast (DIC) microscopy, and were recorded from using patch pipettes filled with a K-gluconate and biocytin based solution. The 127 neurones recorded could be categorized into three subtypes on the basis of their responses to injection of depolarising current pulses; namely tonic firing (type I), burst firing (type II) and spike-adaptive (type III) neurones. Type I interneurones had a higher input resistance, and a lower rheobase than type II neurones. All three neurone subtypes showed "sag" of the voltage response to injection of large amplitude hyperpolarizing current pulses, and, in addition, also showed rectification of the voltage response to injection of depolarising current pulses, with type II neurones showing significantly greater rectification than type I neurones. The axonal arborisations were reconstructed for 44 of 63 neurones labelled with tracer. Neurons of each subtype were found to issue axon collaterals terminating in the brainstem nuclei, including the parvocellular reticular nucleus (PCRt), the trigeminal motor nucleus (Vmot), the supratrigeminal nucleus or the trigeminal mesencephalic nucleus. Twenty-five of the 43 neurones issued collaterals that terminate in the Vmot and the other brainstem nuclei. When viewed under 100x magnification, the collaterals of some interneurones were seen to give off varicosities and end-terminations that passed close to the somata of unidentified neurones in the trigeminal motor nucleus and in the area close to the interneurone soma itself. This suggests that the interneurones may make synaptic contacts on both motoneurones and also on nearby interneurones. These results provide data on the membrane properties of trigeminal interneurones and evidence for their synaptic connections with both nearby interneurones and also with motoneurones. Thus, the interneurones examined could play roles both in the shaping, and possibly also in the generation, of rhythmical signals to trigeminal motoneurones.

Introduction

The trigeminal motor nucleus (Vmot) consists of motoneurones innervating jaw muscles, and is divided into a dorsolateral subnucleus containing jaw-closer (JC) motoneurones and a ventromedial subnucleus containing jaw-opening (JO) motoneurones (Mizuno et al., 1975). The jaw-closer muscles are far bulkier than the jaw-opener muscles and, perhaps not surprisingly, the number of α-motoneurones innervating the jaw-closer muscles far outstrips that innervating the jaw-opener muscles, with the difference being approximately 7:1 in the cat (Rowlerson, 1990). Lateral, and also caudal to the motor nucleus lies a heterogeneous population of interneurones, whose axonal arborisations mainly terminate in the Vmot where they make monosynaptic excitatory and inhibitory synaptic connexions with α-motoneurones (Mizuno et al., 1983; Appenteng et al., 1989; Appenteng et al., 1990; Grimwood et al., 1992; Curtis & Appenteng 1993; Shigenaga et al., 2000; Yoshida et al., 2001). Immunomorphological studies have shown the presence in this area of some neurones immunoreactive for glutamate (Turman & Chandler, 1994a), glutamic acid decarboxylase (GAD), the enzyme that synthesizes γ-aminobutyric acid (GABA; Li et al., 1996), or glycine (Turman & Chandler, 1994b; Li et al., 1996; Rampton et al., 1996), or immunoreactive for GABA and glycine (Yang et al., 1997). This suggests that glutamate may act as the excitatory transmitter, and GABA and glycine as the inhibitory transmitters, at the contacts of these interneurones.

The interneurones in the rostraldorsal part of the trigeminal oral nucleus (oralis-gamma) and adjacent reticular formations (PCRt) receive inputs from muscle and intraoral afferents (Westberg & Olsson, 1991; Westberg et al., 1998), and so are believed to mediate some of the reflex actions of these afferents on motoneurones. It has also been reported that many of the interneurones are rhythmically active during fictive masticatory movements (Landgren & Olsson, 1986; Nozaki et al., 1986a, b; Donga & Lund, 1991; Westberg et al., 1998; Donga, 1999; Westberg et al., 2001), therefore suggesting that they might also transmit some of the centrally generated masticatory rhythm to the motoneurones. In fact, evidence from recent studies (Jacquin et al., 1996; Kogo et al., 1996) suggests that interneurones lying within the area between the trigeminal and facial motor nuclei (Appenteng & Girdlestone, 1987) may be possible candidates for the central pattern generator of rhythmical jaw movements (RJMs; for review see Lund et al., 1998). In support of this, mastication is severely compromised in an animal model in which the third and fifth rhombomeres fail to develop normally (Jacquin et al., 1996).

In spite of their proposed importance in the neuronal circuits of jaw movement control, there have been relatively few studies of the intrinsic membrane properties of interneurones surrounding the Vmot. In a pioneering study, Sandler et al (1998) used the whole cell patch recording method to obtain data on the membrane and firing properties of neurones in the trigeminal main sensory nucleus in the gerbil. More recently, Bourque and Kolta (rat; 2001) have used sharp electrodes to make intracellular recordings from interneurones surrounding the Vmot, including the medial borderzone of the Vmot, supratrigeminal area, intertrigeminal region and PCRt. In the present study we have extended the study of Bourque and Kolta (2001) by focusing on neurones in the area caudal to the Vmot, i.e. the rostral part of the parvocelluar reticular nucleus Alpha (PCRt-α) (Paxinos and Watson, 1998). We have used the whole cell patch recording method to determine the firing patterns and membrane properties of the neurones, and combined this with intracellular labelling of the neurones to determine their quantitative morphology, as well as their axonal trajectories. Such combined data are important for understanding both signal integration in the soma of these neurones, and for an understanding of the neuronal circuits and mechanism by which these neurones influence the control of jaw movements. Preliminary data from this study have been presented in abstract form (Yang et al., 2001).

Methods

Preparation of brain stem slices

The use of animals in this study was in accordance with the rules of the local ethical committee for animal research. Wistar rats aged 5-8 days were anaesthetized with 5% halothane in pure oxygen, and were decapitated. The brain was exposed, chilled with ice-cold artificial cerebrospinal fluid (ACSF), and saggital **brainstem** slices of 300 µm thickness, comprising the Vmot and surrounding regions, were cut with a vibroslicer (Campden, Loughborough, England). The ACSF contained (in mM): NaCl 105, KCl 5, $MgSO_4$ 1.3, $NaHCO_3$ 24, NaH_2PO_4 1.2, $CaCl_2$ 2, and glucose 10; pH adjusted to 7.4 by gassing with 95% O_2 /5% CO_2. The slices were kept in an interface-type chamber at room temperature (24-25°C) to allow recovery for at least 90 minutes.

Visualization of trigeminal interneurones and whole cell patch clamp recording

Slices were transferred to an immersion-type recording chamber mounted to an upright microscope (BX50WI, Olympus Optical Co., Ltd., Tokyo, Japan), equipped with water-immersion objectives, a Normaski optic system, an infrared filter and a CCD camera. Neurones with soma diameter of 10-15 µm and a location caudal to the **Vmot** were visualized, identified and recorded with patch pipettes using procedures described by Stuart *et al*. (1993). Patch pipettes were pulled from borosilicate glass tubing (1.5 mm outer diameter, 0.5 mm wall thickness; Warner Instruments Corp., Hamden, CT, USA), and had a resistance of 5-8 MΩ when filled with internal solution. The internal solution contained (in mM): potassium gluconate 100, EGTA 10, $MgCl_2$ 5, Hepes 40, ATP 3; GTP 0.3; pH adjusted to 7.2 by KOH and osmolarity to 295 mOsm by sucrose. Once the whole cell recordings were obtained, the patch amplifier (Axopatch-1D; Axon Instruments Inc.; Union City, CA, USA) was set to current clamp mode and the bridge was balanced by adjusting the serial resistance compensation of the amplifier. Neurones were only accepted for further study if the membrane potential (Vm) was at least -45 mV without applying holding current, and the spike overshot 0 mV. Signals were low-pass filtered at a corner frequency of 2kHz and then digitized at 10 kHz using a Micro 1401 interface running Signal software provided by CED (Cambridge Electronic Design, Cambridge, UK).

Filling recorded interneurones with biocytin and histology

In a subset of experiments, 10 mM biocytin (Sigma, St. Louis, MO, USA) was included in the internal solution to fill the recorded neurones. Neurones were filled by passive diffusion of biocytin from the patch pipette during the recording period, without application of current. After recording, pipettes were withdrawn and slices left in the recording chamber for additional 30 minutes to allow for biocytin transport within the dendrites and axon. The brain slices were then fixed overnight in 4% paraformaldehyde

(Sigma) in 0.1 M phosphate buffer (PB, pH 7.4) at 4° C. Slices were rinsed with PB several times after fixation and were treated with 3% H_2O_2 in 0.1 M PB for 20 min. Slices were then subjected to histological procedures for visualization of biocytin-filled neurones without further sectioning. They were first incubated in 10% normal goat serum and 0.3% Triton X-100 in phosphate buffered saline (PBS), processed with avidin-biotin horseradish peroxidase complex (ABC, Vector, Burlingame, CA, USA), and finally visualized with 3,3'-diaminobenzidine (DAB) as a chromogen. Biocytin-filled neurones were examined, photographed, and reconstructed with an Olympus BX-50 microscope and a camera lucida drawing tube (SZX-DA, Olympus Optical Co., Ltd., Tokyo, Japan). The drawings of the reconstructed biocytin-filled neurones were digitised using a PC based scanner, and measurements made of soma minimum diameter, soma maximum diameter, dendrite segment length and branching of the axonal collaterals, using NIH-Image software (downloaded from the National Institute of Health website http://www.nih.gov). The soma surface area was determined by assuming an elliptical soma shape, and then calculated as: (major diameter/2) × (minor diameter/2) ×π. All data given are expressed as mean ± standard error, and unless specified, a Mann-Whitney *U*-test was used for statistical comparison.

Results

Under DIC microscopic video with a 10x objective lens, the Vmot could be clearly identified (Fig. 1A1). The Vmot is oval in shape, has a diameter of up to 500 μm, and has fibres, presumably the motor fibres of the 5th nerve, running on its surface. An additional important landmark for the identification of the Vmot is the prominent bundle of fibres of the 7th nerve, located ventral and caudal to the Vmot (see also Curtis & Appenteng, 1993). Following the identification of the Vmot, the visual field was moved to the area caudal to the Vmot (dotted square, Fig. 1A1). By changing to a high power objective lens (40x), a number of neurones with small soma diameter (less than 20 μm) could be clearly identified (Fig. 1A2); whole cell recordings were then made from these neurones. A total of 127 neurones were recorded, of which successful filling with biocytin for precise identification of their location was obtained for 63 neurones, as shown in Fig. 1B. Since the locations of these recorded neurones were outside the borders of the Vmot, and were compatible with the locations of interneurones labelled with transneuronal tracer injected into the jaw-closing muscles (see Appenteng & Girdlestone, 1987; Curtis & Appenteng, 1993), these neurones were presumed to be interneurones.

The firing characteristics of trigeminal interneurones

Based on their firing characteristics, the recorded interneurones can be grouped into three major subtypes, i.e., type I (tonic firing), type II (burst firing), and type III (spike adaptive) interneurones. An example of the response of a type II interneurone to a continuous injection of depolarizing current is shown in Figure 2A. The interneurone fired a train of action potentials (APs) with frequency up to 30 Hz initially upon current injection; the firing frequency then decreased quickly to a more constant level of about 25 Hz (Fig. 2A). The firing of APs was not continuous throughout the period of current injection, but was grouped into bursts that could be separated by periods of several seconds when there was no firing. Interneurones showing this pattern of firing in response to long depolarising current pulses were termed burst firing (or type II) interneurones. The type II interneurones accounted for 41% of all interneurones recorded (52/127), of which 21 interneurones were filled with biocytin and their locations in the slices are shown in Fig. 1B.

The type II interneurones also showed a characteristic of burst firing when a short current pulse (1.5 s) of intensity that was just enough to excite the cell (referred to as rheobase (Rh) hereafter) (Fig. 2B1-i), or even higher (Fig. 2B1-ii), was used, and with the membrane potential (Vm) held at -60 mV. When the interneurones were excited from a resting Vm of -90 mV, only a single or sometimes up to two or three APs, that

were superimposed on a transient slow depolarizing spike, were elicited upon current injection initially (Fig. 2B2-i). After a burst of APs, no further APs were elicited unless the intensity of the current pulse was increased (Fig. 2B2-ii). In some type II interneurones (14/52, i.e. 27%), there was a pronounced transient hyperpolarisation of the interneurone on termination of the current injection (see open arrows in Fig. 2B, cf Fig. 3A), with the amplitude of this hyperpolarisation being dependent on the intensity of the injected depolarizing current pulse (or the amount of prior depolarization). Figure 2C shows the response of a type II interneurone to serial hyperpolarizing and depolarizing current pulses of different intensities, with the recording being made in the presence of 1 μM Tetrodotoxin (TTX) (Fig. 2C1). Note the presence of a prominent sag in the voltage response to injection of large hyperpolarising currents, suggesting the existence of hyperpolarization activated inward current (Ih), and the transient, but slow, depolarisation spike seen following termination of the hyperpolarizing current pulse injection (arrow, Fig. 2C1). Fig 2C2 shows, for combined data from 4 type II interneurones, the plot of current against the change in membrane potential (i.e. *I-ΔVm*) for both injections of depolarising and hyperpolarizing current pulses. The plot reveals a shallower slope of the *I-ΔVm* plot for depolarising as opposed to hyperpolarizing current injection (Fig.2C2, star), indicating rectification in the response to depolarising current injection (i.e. depolarising rectification).

Figure 3A shows a recording made from another type II interneurone. The firing pattern of this interneurone shifted from burst firing to continuous firing upon changing the perfusion medium from normal ACSF (Fig. 3A, column a1) to Ca^{++} free ACSF (Fig. 3A, column a2). Superimposition of the recordings revealed that in Ca^{++} free ACSF, that the time course of depolarization of Vm upon current injection became faster, that the depolarization following the AP was blocked (Fig. 3A, column a1+a2), and that the interneurone fired faster and more regularly (Fig. 3A, column a1+a2). These results suggested that the burst firing characteristic of type II interneurones is calcium-dependent. Furthermore, the transient, slow spike evoked by depolarization (Fig. 3B, b1), and at the termination of a hyperpolarizing pulse, in normal conditions was also blocked upon application of Ca^{++} free ACSF (Fig. 3B, b2), suggesting a Ca^{++} current mediated response. Figure 4 shows the effect of calcium on the firing pattern of type II interneurone. Note the change of the burst firing pattern to a continuous firing pattern upon perfusion of Ca^{++} free ACSF (Fig. 4), and the change back after the return to a normal ACSF solution.

In contrast to type II interneurones, the type I interneurones showed tonic firing in response to injection of a depolarizing current pulse of long duration (Figure 5A), with the firing frequency increasing with increasing amount of current injection, and firing to

a given level of current injection showing only little adaptation. A total 62 (49%) interneurones showed such firing characteristics, and these were classified as tonic firing (type I) interneurones. Among the recorded type I interneurones, 35 interneurones were filled with biocytin and their locations in slices are shown by grey circles in Fig. 1B. When a depolarizing current pulse with intensity of Rh was injected, only a single AP, followed by an afterhyperpolarization (AHP), was elicited with the Vm held at either -65 (Fig. 5B1) or -100 mV (Fig. 5B2). Using higher intensities, a train of APs with regular intervals was elicited with the Vm held at either -65 (Fig. 5B1, lower trace) or -95 mV (Fig. 5B2, lower trace). Figure 5C shows, for another type I neurone, the voltage response to injection of current pulses of varying intensities, with the recording made with the addition of TTX in the ACSF (Fig. 5C1). Note the prominent sag in the voltage response to hyperpolarizing current injection (arrow, Fig. 5C1), suggesting, as with type II interneurones, the presence of Ih in type I interneurones. However, in contrast to type II interneurones, there was no transient depolarising spike seen at the termination of the current injection. Figure 5C2 shows the combined *I-ΔVm* plot for 4 type I interneurones recorded under the same conditions. Comparison of the mean slopes of the current-voltage relationship, using data points obtained in response to depolarising and hyperpolarisng current injection, gave mean ratio of 0.68 ±0.09 and 0.33±0.05 for type I and II neurones respectively ($p<0.05$), indicating a less pronounced rectification of the response for type I than for type II interneurones (cf. Figs 2C & 5C).

The type III interneurones are so named as, in response to long depolarising current pulses at intensities above Rh, they fire just a few APs and then cease firing (Fig. 6A). Unlike type II interneurones, the few spikes fired were not superimposed on a transient slow depolarising spike (Fig. 6A). However, the interneurones could fire additional APs if the intensity of the on-going current injection was increased (Fig. 6 A, open arrows). Interneurones with this firing pattern were termed spike-adaptive (type III) interneurones, and their population accounted for 10% (13/127) of all interneurones recorded, of which 7 interneurones were filled with biocytin and are shown in open triangles in Fig. 1B. Type III interneurones fire a single AP with no delay upon injection of a depolarizing current pulse of duration 1.5s and with intensity of Rh (Fig. 6B1, top trace). The interneurones show a rapid adaptation of firing to the stimulation, and use of higher intensities of depolarizing current pulse could not elicit a train of APs (Fig. 6B1, lower trace). A similar phenomenon was seen when the Vm was held at -90 mV (Fig. 6B2). Figure 6C shows the response of the Vm of another type III interneurone to serial hyperpolarizing and depolarizing current pulses of different intensities (Fig. 6C1), with the plot of *I-ΔVm* being shown in Fig. 6C2. Note as with type I and type II interneurones the presence of sag in the voltage response to hyperpolarizing currents (Fig.6C1), and the depolarisation rectification evident in Fig.6C2. As with type II

interneurones, but in contrast to type I interneurones, type III interneurones showed a transient, but slow depolarisation spike, following the termination of injection of a hyperpolarizing current pulse (Fig. 6C1, arrow). This depolarisation spike is presumably a Ca^{++} mediated response though we did not test its ionic mechanism.

The membrane properties of trigeminal interneurones

The resting Vm of all the three types of interneurones was about -50 mV (Table 1). The type I interneurones fired spontaneously, and regularly, at 7.5±6.2 Hz (n=21) at resting Vm, and to prevent spontaneous firing, application of a little hyperpolarizing current to hyperpolarize Vm to more than -60 mV was necessary. In contrast, type II and type III interneurones were silent at resting Vm. Table 1 summaries the membrane properties of the three classes of interneurones, and Fig. 7 illustrates how these properties were calculated with Vm held at –60 ~ -65 mV, including the input resistance (Rn) (Fig. 7A), membrane time constant (τ) (Fig. 7B), sag (Fig. 7C), and AHP (Fig. 7D). For Rn, a significant difference between type I and type II interneurones was noticed ($p<0.02$). Consistent with this difference in Rn, Rh of type II interneurones was significantly higher than that of type I interneurones ($p<0.005$). Values of Rn and Rh of type III interneurones were not significantly different from those of type I and type II interneurones, possibly due to a small number of type III interneurones recorded. For τ and sag, no significant difference was found between type I, type II and type III interneurones (see Table 1). Two forms of AHP, i.e. mono- and bi-phasic (see Fig. 7E), were found in interneurones of all types. The amplitude of the fast AHP, and both the amplitude and half decay of the slow AHP, were not significantly different between type I and type II interneurones. The same held true for type III interneurones, with the exception that the amplitude of the slow AHP was significantly smaller in type III than in either type I or type II interneurones (Table 1). The parameters of spike shape, including amplitude and half width, were not significantly different among the three interneurone types.

Morphology of trigeminal interneurones

Table 2 summarises the quantitative data on the soma and dendritic morphology of interneurones filled with biocytin (n=63), with parenthesis showing data from neurones having axonal arborisations that gave end-terminations, or varicosities, within the Vmot. The major (or maximum) soma diameter of type I interneurones was significantly smaller than that of type II interneurones, but minimum soma diameters and the soma surface areas of the three types of interneurones were not significantly different. Similarly, there were no significant differences in the mean dendritic segment length, mean dendritic path length, mean number of dendrites per interneurone, or the and mean number of terminals per dendrite of the three types of interneurones (Table 2). The

proportions of all segments forming end-terminals in each segment were not significantly different for the three interneurone types (Kolmogorov-Smirnov test; table 2). The second, third and fourth order dendritic segments accounted for up to 60% of end-terminals per dendrite, suggesting that most dendrites of all three interneurone types branch only 2 or 3 times (Table 2). Taken together, the above results suggest that the dendritic patterns of the three types of interneurones are very similar and are relatively simple compared to those of motoneurones (see Min & Appenteng, 1996).

Fig. 8 shows the reconstruction of the morphology of a type II interneurone. The neurone had an oval soma and 3 primary dendrites (Fig. 8& insert c). The axon was found to give off collaterals close to the soma of the interneurone (Fig.8). The axon coursed mostly in the dorsal-rostral direction, and arborised extensively within the Vmot (Fig.8 & inserts b & d). Under 100x magnification, many swollen varicosities and end-terminations could be clearly identified within the Vmot (Fig.8 insert d), with some of these being in close proximity to unidentified cells in the Vmot. Similar, varicosities and end-terminations were also found on collaterals that arborised in the PCRt-α, with some of these again being in close proximity to the soma of unidentified cells (Fig. 8, insert e). The varicosities and end-terminations suggest possible sites of synaptic contact, with some of these sites being on the soma of cells in the two regions. Fig. 9 shows the reconstruction of a type I interneurone. The axon of the interneurone appeared to bifurcate, with one branch heading rostrally to the Vmot, where it arborised extensively, and the other heading caudally for some distance. In addition, there were extensive collateral arborisations within the PCRt-α, in the region close to the location of the interneurone soma. Varicosities and end-terminations could be identified on some collaterals, with some of these being in close proximity to cells in the Vmot (insert c), PCRt-α (insert d) , and also further caudally (insert e).

We were able to obtain reconstructions of the axonal trajectories of 43 interneurones. The axons were mostly directed rostro-ventrally, rostro-dorsally (Fig. 10c), and ventro-caudally (Fig. 10b), and in some cases the axons could be traced to the level of the midbrain or of the upper cervical spinal cord. We found only two interneurones whose axonal branches were directed in the dorso-caudal direction. Overall, we could find no systematic differences in the axonal branching of type I and type II interneurones, but it appeared that the axons of type II interneurones were directed more ventrally than those of type I interneurones. In addition to giving off collateral branches in the PCRt-α, most of the interneurones (25/43) also gave off collaterals within the Vmot (Figs. 8, 9, 10a). The axons of 6/43 interneurones appeared to course towards the trigeminal mesencephalic nucleus (Vme; Fig. 10c), while the axons of 6/43 coursed towards the lower brainstem (e.g. Fig. 10b). Some of the interneurones appeared to have

multiple sites of projection in that 5/43 (3 type I, 2 type II) projected to both the Vmot and Vme, 5/44 (4 type I, 1 type II) to both the Vmot and lower brain stem, 2/44 (1 type I, 1 type II) to the Vme and lower brain stem, and 3/44 (1 type I and 1 type II) to the Vmot, Vme and the lower brain stem. However, for 20/63 interneurones, no obvious axonal arborisation were seen, possibly because their principal axon had been cut off during preparation of the slice.

Discussion

In this study, we have made use of whole cell recording techniques to obtain intracellular recordings from interneurones lying caudal to the Vmot. The recorded interneurones had distinct firing properties, and based on these properties we grouped these interneurones into three subtypes, i.e. tonic firing (type I), bursting firing (type II) and spike-adaptive (type III) interneurones. In general, all three types of neurones showed some degree of sag in their voltage response to hyperpolarizing currents and some rectification in the voltage response to depolarising current pulses, though the latter was more pronounced for type II than for type I interneurones. In addition, type II and type III interneurones, but not type I interneurones showed a transient, but slow depolarisation spike, following the termination of injection of a hyperpolarizing current pulse. With the exception of Rn and Rh, which were found to be significantly different in type I and type II interneurones, the passive membrane properties and morphology, including axonal and dendritic branching patterns, were not significantly different among the type I, type II and type III interneurones. The findings that each subtype of the interneurones issues axon collaterals terminating in the Vmot and the PCRt suggest that neurones in PCRt play an important role for the generation of distinct mastication patterns by acting directly or indirectly on motoneurones.

Unit identification

The neurones recorded in this study were located in the area between the caudal border of the Vmot and the rostral border of the facial motor nucleus (see Fig. 1). The major nucleus included within this area is the PCRt-α (Paxinos & Watson, 1998), a region known to contain interneurones for trigeminal motoneurones. Both the electrical properties and morphology of these interneurones were different from that previously reported for motoneurones in a study in which similar recording methods were used in slices from animals of the same age (Min and Appenteng, 1996). For example, the Rn and ι determined for interneurones in the present study were more than 4-5 fold greater than that reported for motoneurones (Rn: 161±227 MΩ; ι: 8.62±1.48 ms; see Table 1 of Min and Appenteng, 1996). In addition, motoneurones had larger soma diameters (about 35 μm), more averaged terminals per dendrite (11 terminals on average), more complex dendritic branching patterns (the 4th, 5th and 6th orders of segments accounting for most end-terminals in motoneurones), and shorter average dendritic segment lengths (cf. Table 2 of Min & Appenteng, 1996 to Table 2 of this study). Finally, the firing patterns of all the three subtypes of interneurones recorded in the present study were different from those of motoneurones. Taken together, the data clearly indicates that the present recordings were indeed obtained from interneurones. The axonal reconstructions made allowed some of the sites of projection of these interneurones to be identified. Most interneurones projected to both the PCRt-α and the Vmot, while others appeared to

project to the Vme and to areas caudal to the PCRt-α, with some appearing to project to multiple sites. However, the data does allow us to infer that the majority of interneurones studied may exert synaptic actions both on other interneurones, possibly including other premotor neurones, as well as on motoneurones. This does not of course preclude actions on other neurones that could not be adequately examined possibly due to the limitations of the slice preparation. We therefore consider that the present data provides further support for earlier reports that interneurones in this area make synaptic contacts with α-motoneurones in the Vmot (Appenteng et al., 1989, 1990; Shigenaga *et al*., 2000; Yoshida *et al*., 2001).

Firing properties of interneurones

In their pioneering study on neurones in the trigeminal main sensory nucleus of the gerbil, Sandler et al (1996) reported three subtypes of neurones based on the response to injection of depolarising current pulses. Neurones they termed bursters showed, as in the present study, a similar burst of spikes superimposed on a slow depolarisation, followed by subsequent firing at a slower rate. Similarly, the burster neurones reported in the two studies showed, in response to hyperpolarizing current pulses, sag and rebound firing on the termination of the current pulse. However, Sandler et al (1996) reported that burster neurones could show, in response to depolarising currents, "an oscillatory burst of three or four action potentials with decreasing peak amplitudes until the potential plateaued for a variable period" (i.e. plateau burst). Such responses were reported to be rare in slices bathed in normal ACSF but consistent in slices bathed in either zero calcium with addition of calcium channel blockers, or simply in zero calcium ACSF without the addition of calcium channel blockers (Sandler et al 1996). We did not observe plateau potentials in the present study, even though some burster interneurones (n = 5) were also studied in zero calcium ACSF. Indeed, we found that when bathed in zero calcium ACSF, the characteristic firing of burster interneurones was replaced by firing more reminiscent of that of type I interneurones. This difference may reflect a possible heterogeneity in properties of burster interneurones, either related to the location of the interneurones (SupV cf PCRt-α), or a species or developmentally related difference in bursters (gerbil cf rat; Sandler et al, 1996). Sandler et al (1996) described an additional two groups of neurones that did not show bursts but which fired tonically to depolarising currents. One group of tonic neurones showed both sag and rebound firing in response to hyperpolarizing current pulses, while the other did not show either of these responses. The presence of both tonic firing and sag in the former group of interneurones are properties shared by the type I interneurones reported here. However, the rebound firing on termination of the current pulse was only occasionally found in the present sample of type I interneurones. Also, the absence of sag in the latter group of interneurones was not a feature shown by our

type I interneurones. It would also appear that type III were not present in the sample reported by Sandler et al (1996). The properties of the three neuronal subtypes reported in this study are broadly similar to those reported earlier by Bourque and Kolta (2001). The firing, in response to depolarising current pulses, of both types I and type III interneurones were identical to that reported here. Furthermore, both type I and type III interneurones were reported to show sag and depolarisation rectification (Bourque and Kolta, 2001). The type II interneurones identified by Bourque and Kolta (2001) like those reported in this study, showed cessation of firing during a depolarising pulse. However, the type II interneurones recorded by Bourque and Kolta (2001), unlike those recorded in the present study, did not show spikes superimposed on a transient slow depolarizing spike at the onset of firing to depolarising pulses. It is possible the greater sensitivity of the patch recording method, as opposed to that of sharp electrodes, may have allowed such depolarising spikes to be revealed. It is worth noting that values of spike amplitude and Rn obtained in the present study were respectively 2.5 and 15 fold greater than those reported by Bourque and Kolta (2001), this being in line with differences of similar magnitude reported in comparisons of data obtained with patch and sharp electrodes in other systems (Spruston and Johnson, 1992; Spruston et al., 1994; Min and Appenteng, 1996).

The distinct discharge patterns of the three neuronal types suggest that the ionic mechanisms underlying APs and firing patterns may differ among the different subtypes of interneurones. The most significant difference between type II (or III) and type I is in the Ca^{2+}-spikes induced by depolarization. This Ca^{2+}-spike might be mediated by a low threshold voltage-dependent calcium channel (LTVDCC), as it could also be activated by re-depolarization of Vm upon cessation of the hyperpolarizing current pulse injection (Llinas *et al*., 1992; Calabrese, 1998). Calcium influx through these channels may in part account for the phasic firing pattern of type II interneurones, because type II interneurones could fire continuously in Ca^{2+} free ACSF (4 out of 5 cells tested; see Fig. 3). The calcium current mediated by LTVDCC is often referred as I_t (low threshold transient Ca^{2+} current) (Steriade *et al*., 1993; Luithi & McCormick, 1998a, b). In mammalian thalamicortical neurones, it has been reported that interplay between I_t and I_h has an important role in generation of rhythmical oscillations during non-REM (rapid eye movement) sleep. It is therefore likely that other cationic currents, in particular the potassium current (Sah, 1996) or/and perhaps I_h as well, activated by intracellular Ca^{2+} influx through LTVDCC may contribute to the phasic discharging pattern of type II interneurones and spike adaptive characteristic of type III interneurones. Nevertheless, further detailed pharmacological data is needed to support the above suggestion. Although interneurones recorded in this study could be clearly grouped based on their firing patterns (see also Bourque & Kolta, 2001), further more precise and detailed

classification of each subtype on other physiological and morphological criteria are necessary. For instance, a long lasting AHP induced by a train of APs elicited by depolarizing current pulse (Fig.2B, open arrows) was only found in a subpopulation of type I interneurones, and an AHP following a single AP elicited by a short, but high intensity, depolarizing current pulse was biphasic in some interneurones, but monophasic in others within the same subtype (see Table 1).

Functions of trigeminal interneurones.

It was previously accepted that the central pattern generator for rhythmical jaw movements was located in the bulbar reticular formation (Dellow & Lund, 1971; Chandler & Goldberg, 1982; Nozaki *et al*., 1986a, b; Chandler & Goldberg, 1988). It was proposed that neurones in these areas relay inputs from the cortex and trigeminal afferents by monosynaptically exciting neurones in a more dorso-medial neuronal group to establish the masticatory rhythm (for Review see Lund *et al*., 1998). Recent evidence (Jacquin *et al*., 1996; Kogo *et al*., 1996), however, argues that the groups of neurones involved in the genesis of the masticatory patterns are located more rostral than previously reported, and within a critical area between the trigeminal and facial motor nuclei (see Lund *et al*., 1998). This is exactly the area where our recorded interneurones were located, raising the possibility that the interneurones recorded in this study may be involved in the generation of the masticatory rhythm. In Rpc-α many interneurones are phasically activated while a small number of interneurones are tonically activated, during fictive masticatory movements elicited by cortical stimulation (Donga & Lund, 1991; Westberg *et al*., 1998; Westberg *et al*., 2001). In this study, the recorded interneurones had similar discharge patterns when they were activated by continuous injection of depolarizing currents, raising the possibility that they may belong to the same population of interneurones as those recorded in vivo studies in different species (Westberg *et al*., 1998; Westberg *et al*., 2001).

However, it would appear unlikely that the type II interneurones recorded in this study could, by themselves, indeed act as the CPG for fictive masticatory movements as, apart from the bursts being very irregular in frequency and duration, the interenruones did not show some of the features reported for neurones that are rhythmically active during fictive movements. For example, the type II interneurones recorded here did not show a negative slope region of the steady *I-V* plot, or so called Na^+ current mediated plateau potential, on which bursts of spikes are superimposed in certain neurone types, including spinal interneurones activated during locomotion in rats (Kiehn et al, 1996) and neurones in the trigeminal main sensory nucleus (Sandler et al, 1996). The trigeminal main sensory nucleus has recently been considered as a CPG for fictive masticatory movements as neurones in the nucleus were found to fire in phase with the

fictive motor program (Tsuboi et al, 2003). The key evidence required to determine if type-II neurones are involved in the CPG for fictive masticatory movements would be to assess if they could fire in phase with the fictive motor program. Unfortunately, this is very difficult to perform in the slice preparation used in this study. We can not dismiss the possibilities that the features of irregular firing frequency and duration of the present type-II neurones might stem from the type of preparations used, in which many neuronal circuits were cut off, or possibly stem from the use of immature animals for our experiments.

In addition to intrinsic membrane potential fluctuations, rhythmical activity can be produced as a result of interactions of between populations of excitatory and inhibitory cells that make reciprocal connections with each other (Inoue *et al*., 1994.). Interestingly, of the 25/43 interneurones with projections to both the PCRt-α and the Vmot, 60% were type-I interneurones and 36% type-II interneurones. The synaptic actions and the neurotransmitters associated with the different types of interneurones remain to be determined. During cortically induced fictive mastication, jaw-closer motoneurones show EPSPs (excitatory postsynaptic potentials) during the fictive jaw-closing phase and IPSPs (inhibiroty postsynaptic potentials) during the jaw-opening phase. In contrast, jaw-opener motoneurones show EPSPs during the jaw-opening phase but no IPSPs during the jaw-closure phase (Nozaki *et al*., 1993). The immunohistochemical evidence suggests the presence of four functional groups of interneurones in the PCRt-α; neurones containing glutamate (Turman & Chandler, 1994a), neurones containing GABA (Li *et al*., 1996), neurones containing glycine (Turman & Chandler, 1994b; Li *et al*., 1996; Rampton *et al*., 1996), and neurones containing both GABA and glycine (Yang *et al*., 1997). Identification of the neurotransmitters present in the different subtypes of interneurones is clearly of importance to assessment of the roles played by the interneurones in mastication. However, the present data provides evidence that the interneurones studied here can contribute to the control of masticatory movements by monosynaptic actions on motoneurones and other interneurones, including possibly other premotor neurones. In addition, the projection to the Vme of some interneurones supports the suggestion (Westberg & Olsson, 1991; Westberg *et al*., 1998) that some interneurones in PCRt-α may be involved in coordinating sensory and masticatory motor commands. Finally, the projection of some interneurones to the lower brainstem or upper cervical spinal cord suggests that some interneurones PCRt-α may coordinate masticatory movements with other motor controls, e.g. respiratory rhythm and control of muscles responsible for the movements of neck and forelimbs relating to feeding behaviour.

Acknowledgements

We are grateful to Drs. K. Appenteng and T. F.C. Batten for their reading of and helpful comments on the manuscript. This work was supported by grants from National Science Council, Taiwan (NSC 91-2320-B-040-021 & NSC 91-2320-B039-007) and China Medical University (CMC-91-M-10). C.-T. Wang was involved in reconstruction of some interneurones.

Abbreviations

τ, membrane time constant; ACSF, artificial cerebrospinal fluid; AHP, afterhyperpolarization; APs, action potentials; CPG, central pattern generator; GABA, γ-aminobutyric acid; I-ΔVm, current against the change in membrane potential; Ih, inward current; IR-DIC, infrared differential interference contrast; PCRT-α, parvocellular reticular formation alpha; PCRt, parvocellular reticular formation; Rh, rheobase; Rn, input resistance; TTX, tetrodotoxin; Vm, membran potential; Vme, trigeminal mesencephalic nucleus; Vmot, trigeminal motor nucleus.

References

Appenteng, K., Conyers, L. & Moore, J.A. (1989) The monosynaptic excitatory connections of single trigeminal interneurones to the V motor nucleus of the rat. *J. Physiol*., **417**, 91-104.

Appenteng, K., Conyers, L., Curtis, J.C. & Moore, J.A. (1990) Monosynaptic connexions of single trigeminal interneurons to the contralateral V motor nucleus in anaethetised rats. *Brain Res*., **514**, 128-130.

Appenteng, K. & Girdlestone, D. (1987) Transneuronal transport of wheat germ agglutinin-congugated horseradish peroxidase into trigeminal interneurones of the rat. *J. Comp. Neurol*., **258**, 387-386.

Blanton, M.G., LoTurco, J.J. & Kreigstein, A.R. (1989) Whole cell recording from neurons in slices of reptilian and mammalian cerebral cortex. *J. Neurosci. Methods,* **30**, 203-210.

Bourque, M.J. & Kolta, A. (2001) Properties and interconnections of trigeminal interneurons of the lateral pontine reticular formation in the rat. *J. Neurophysiol*., **86**, 2583-2596.

Calabrese, R. (1998) Cellular, synaptic, network, and modulatory mechanisme involved in rhythm generation. *Curr. Opin. Neurobiol*., **8**, 710-717.

Chandler, S.H. & Goldberg, L.J. (1982) Intracellular analysis of synaptic mechanisms controlling spontaneous and cortically induced rhythmical jaw movements in the guinea pig. *J. Neurophysiol*., **48(1)**, 126-38.

Chandler, S.H. & Goldberg, L.J. (1988) Effects of pontomedullary reticular formation stimulation on the neuronal networks responsible for rhythmical jaw movements in the guinea pig. *J. Neurophysiol*., **59(3)**, 819-32.

Curtis, J.C. & Appenteng, K. (1993) The electrical geometry, electrical properties and synaptic connection onto rat V motoneurones in vitro. *J. Physiol*., **465**, 85-119.

Dellow, P.G. & Lund, J.P. (1971) Evidence for central timing of rhythmical mastication. *J. Physiol*., **215(1)**, 1-13.

Donga, R. (1999) Are trigeminal premotor interneurones part of the masticatory central pattern generator? In Nakamura, Y. & Sessle, B.J. (eds), *Neurobiology of Mastication:*

From Molecular to Systems Approach. Elsevier Science, pp. 277-298.
Donga, R. & Lund, J.P. (1991) Discharge patterns of trigeminal commissural last-order interneurones during fictive mastication in the rabbit. *J. Neurophysiol*., **66**, 1564-1578.

Fay, R.A. & Norgren, R. (1997) Identification of rat brainstem multisynaptic connections to the oral motor nuclei in the rat using pseudorabies virus II. Facial muscle and motor system. *Brain Res. Rev*., **25**, 255-275.

Grimwood, P.G., Appenteng, K. & Curtis, J.C. (1992) Monosynaptic EPSPs elicited by single interneurones and spindle afferents in trigeminal motoneurones of anaesthetized rats. *J. Physiol*., **455**, 641-662.

Jacquin, T.D., Borday, V., Schneider-Maunoury, S., Topilko, P., Ghilini, G., Kato, F., Charnay, P. & Champagnat, J. (1996) Reorganization of pontine rhythmogenic neuronal networks in Krox-20 knockout mice. *Neuron*, **17**, 747-758.

Kiehn, O., Johnson, B.R. & Raastad, M. (1996) Plateau properties in mammalian spinal interneurons during transmitter-induced locomotor activity. *Neuroscience*, **78(1),** 263-273.

Kogo, M., Funk, G.D. & Chandler, S.H. (1996) Rhythmical oral-motor activity recorded in an in vitro brainstem preparation. *Somatosens. Motor Res*., **13**, 39-48.

Kolta, A. (1997) In vitro investigation of synaptic relations between interneurons surrounding in trigeminal motor nucleus and masseteric motoneurons. *J. Neurophysiol*., **78**, 1720-1725.

Kolta, A., Westberg, K.G. & Lund, J.P. (2000) Identification of brainstem interneurons projecting to the trigeminal motor nucleus and adjacent structures in the rabbit. *J. Chem. Neuroanat*., **19**, 175-196.

Landgren, S. & Olsson, K.A. (1986) Bulbar neurones with axon projections to the trigeminal motor nucleus in the cat. *Exp. Brain Res*., **65**, 98-111.

Li, Y.-Q., Takada, M., Kaneko, T. & Mizuno, T. (1996) GABAergic and glycinergic neurons projecting to the trigeminal motor nucleus: a double labeled study in the rat. *J. Comp. Neurol*., **373**, 498-510.

Llinas, R., Sugimori, M., Hillman, D.E. & Cherksey, B. (1992) Distribution and

functional significance of the P-type, voltage-dependent Ca^{2+} channels in the mammalian central nervous system. *Trends. Neurosci*., **15**, 351-355.

Luithi, A. & McCormick, D.A. (1998a) Periodicity of thalamic synchronized oscillation: the role of Caz+-mediated upregulation of I_h. *Neuron*, **20**, 553-563.

Luithi, A. & McCormick, D.A. (1998b) H-current: properties of a neuronal and network pacemaker. *Neuron*, **21**, 9-l 2.

Lund, J.P., Kolta, A., Westberg, K.G. & Scott, G. (1998) Brainstem mechanisms underlying feeding behaviors. *Curr. Opin. Neurobiol*., **8(6)**, 718-24.

Min, M.-Y. & Appenteng, K. (1996) Multimodal distribution of amplitude of miniature and spontaneous EPSPs recorded in rat trigeminal motoneurones. *J. Physiol*., **494**, 171-182.

Mizuno, N., Konishi, A. & Sato, M. (1975) Localization of masticatory motoneurons in the cat and rat by means of retrograde axonal transport of horseradish peroxidase. *J. Comp. Neurol*., **164**, 105-116.

Mizuno, N., Yasui, Y., Nomura, S., Itoh, K., Konishi, A., Takada, M. & Kudo, M. (1983) A light and electron microscopic study of premotor neurons for the trigeminal motor nucleus. *J. Comp. Neurol*., **215**, 290-298.

Nozaki, S., Iriki, A. & Nakamura, Y. (1986a) Role of corticobulbar projection neurons in cortically induced rhythmical masticatory jaw-opening movement in the guinea pig. *J. Neurophysiol*., **55(4)**, 826-45.

Nozaki, S., Iriki, A. & Nakamura, Y. (1986b) Localization of central rhythm generator involved in cortically induced rhythmical masticatory jaw-opening movement in the guinea pig. *J. Neurophysiol*., **55**, 806-825.

Paxions, G. & Watson, C. (1998) *The rat brain in stereotaxic coordinates.* Academic Press, San Diego.

Rampon, C., Peyron, C., Petit, J.M., Fort, P., Gervasoni, D. & Luppi, P.H. (1996) Origin of the glycinergic innervation of the rat trigeminal motor nucleus. *Neuroreport*, **7(18)**, 3081-3085.

Rowlerson, A.M. (1990) Specialization of mammalian jaw muscles: Fibre type compositions and the distribution of muscle spindles. In Taylor, A. & Publ, A. (eds),

Neurophysiology of the Jaws and Teeth. Mcmillan Press Ltd, London, pp. 1-51.

Ruscheweyh, R. & Sandkühler, J. (2002) Lamina-specific membrane and discharge properties of rat spinal dorsal horn neurones *in vitro*. *J. Physiol*., **541**, 231-244.
Sandler, V.M., Puil, E. & Schwarz, D.W.F. (1998) Intrinsic response properties of bursting neurons in the nucleus principalis trigemini of the gerbil. *Neuroscience,* **83(3),** 891-904.

Sah, P. (1996) Ca^{2+}-activated K^{+} currents in neurones: types, physiological roles and modulation. *Trends Neurosci*., **19**, 150-154.

Shigenaga, Y., Hirose, Y., Yoshida, A., Fukami, H., Honma, S. & Bae, Y.C. (2000) Quantitative ultrastructure of physiologically identified premotoneuron terminals in the trigeminal motor nucleus in the cat. *J. Comp. Neurol*., **426(1)**, 13-30.

Spruston, N. & Johnston, D. (1992) Perforated patch-clamp analysis of the passive membrane properties of three classes of hippocampal neurons. *J. Neurophysiol*., **67**, 508-529.

Spruston, N., Jaffe, D.B. & Johnston, D. (1994) Dendritic attenuation of synaptic potentials and currents: the role of passive membrane properties. *Trends Neurosci*., **17(4),** 161-166.

Steriade, M., McCormick, D. & Sejnowski, T. (1993) Thalamocortical oscillations in the sleeping and aroused brain. *Science*, **262**, 679-685.

Stuart, G.J., Dodt, H.U. & Sakmann, B. (1993) Patch-clamp recordings from the soma and dendrites of neurons in brain slices using infrared video microscopy. *Pflügers Arch*., **423**, 511-518.

Tsuboi, A., Kolta, A., Chen, C.C. & Lund, J.P. (2003) Neurons of the trigeminal main sensory nucleus participate in the generation of rhythmic motor patterns. *Eur. J. Neurosci*., **17**, 229-238.

Turman, J.J. & Chandler, S.H. (1994a) Immunohistochemical localization of glutamate and glutaminase in guinea pig trigeminal premotoneurones. *Brain Res*., **634**, 49-61.

Turman, J.J. & Chandler, S.H. (1994b) Immunohistochemical evidence for GABA and glycine containing trigeminal premotoneurons in the guinea pig. *Synapses*, **18**, 7-20.

Westberg, K.G., Clavelou, P., Sandstrom, G. & Lund, J.P. (1998) Evidence that trigeminal brainstem interneurons form subpopulation to produce different forms of mastication in the rabbit. *J. Neurosci*., **18**, 6466-6479.

Westberg, K.G. & Olsson, K.A. (1991) Integration in trigeminal premotor interneurones in the cat 1: functional characteristics of neurones in the subnucleus-γ of the oral nucleus of the spinal trigeminal tract. *Exp. Brain Res*., **84**, 1102-1114.

Westberg, K.G., Sandstrom, G. & Olsson, K.A. (1995) Integration in trigeminal premotor interneurones in the cat 3: input characteristics and synaptic action of neurones in subnucleus-γ of the oral nucleus of the spinal trigeminal tract with a projection to the masseteric motoneurone subnucleus. *Exp. Brain Res*., **104**, 449-461.

Westberg, K.G., Scott, G., Olsson, K.A. & Lund, J.P. (2001) Discharge patterns of neurons in the medial pontobulbar reticular formation during fictive mastication in the rabbit. *Eur. J. Neurosci*., **14**, 1709-1718.

Yang, H.-W., Chen, S.-H. & Min, M.-Y. (2001) The electrical and morphological properties of interneurons lying dorsal caudal to the rat trigeminal motor nucleus. *Society for Neuroscience Abstract*, **27**, 295.4.

Yang, H.-W., Min, M.-Y., Appenteng, K. & Batten, T.F.C. (1997) Glycine-immunoreactive terminals in the rat trigeminal motor nucleus: light- and electron-microscopic analysis of their relationships with motoneurones and GABA-immunoreactive terminals. *Brain Res*., **749**, 301-319.

Yoshida, A., Yasuda, K., Dostrovsky, J.O., Bae, Y.C., Takemura, M., Shigenaga, Y. & Sessle, B. (1994) Two major types of premotoneurons in the feline trigeminal nucleus oralis as demonstrated by intracellular staining with horseradish peroxidase. *J. Comp. Neurol*., **347**, 495-514.

Yoshida, A., Fukami, H., Nagase, Y., Appenteng, K., Honma, S., Zhang, L,F., Bae, Y.C. & Shigenaga, Y. (2001) Quantitative analysis of synaptic contacts made between

functionally identified oralis neurons and trigeminal motoneurons in cats. *J. Neurosci*., **21(16)**, 6298-307.

Figure Legends

Figure 1. Identification of interneurones and distribution of biocytin labelled interneurones in saggital brainstem slices.

A. Trigeminal motor nucleus (Vmot) and the seventh nerve (7n) viewed using IR-DIC microscopy video with 10x objective lens (A1). The dotted square indicates area within which interneurones were recorded. When the area is magnified by using a 40x objective lens, neurones with small soma diameters could be clearly identified and recorded (A2, arrows). *B.* Schematic diagram shows the distribution of all neurons labelled with biocytin. The outlines of the Vmot, 7n (7th nerve) and VIImot (facial motor nucleus) are shown by the dotted lines. **D, dorsal; C, caudal.** Scale bar= 200 μm (A1), 25 μm (A2).

Figure 2. Recordings made from type II neurones.

A. The type II neurone was silent at Vm = -61 mV, and displays burst firing in response to a prolonged, steady, depolarising current pulse (upper trace). Middle trace shows the firing frequency analysed using mini-analysis software of Synatosoft (USA) and lower trace shows the injected current. *B1.* The type II neurone also displays burst firing to injection of a 1.5 s depolarizing current pulse with the Vm held at around ~-60 mV (horizontal arrows). Upper (i) and middle (ii) traces are the neuronal response to injected current pulses with intensity of Rh and 2*Rh respectively. Lower trace shows superimposed traces of the injected current pulses. *B2.* With Vm being hyperpolarized to ~-90mV, a Ca^{2+} mediated spike was evoked followed by a burst of APs (i and insert). Higher current intensity elicits trains of APs with irregular intervals (ii). Note the afterhyperpolarization (AHP) following the termination of current injection (see **arrows**). Lower trace shows superimposed traces of injected current pulses. *C1.* Superimposed Vm responses (upper traces) to hyperpolarising and depolarising current pulses (lower traces). TTX was added to the ACSF and the Vm held at ~-60mV. Note the evoked Ca^{2+} spike following the termination of the hyperpolarising current pulses (arrow). *C2.* Plot of Vm change against the intensity of current injection for 4 type I neurones. **The star marks the region of rectification to depolarising current pulses.**

Figure 3. Burst firing characteristic of type II neurones is Ca^{2+}-dependent.
A. A type II neurone recorded in normal ACSF (a1), Ca^{2+} free ACSF, and superimposed responses of a1 (black) and a2 (grey) shown in larger scale. The Vm was held at ~-100mV (see horizontal arrows). Upper traces are responses to 90 pA and lower traces

are response to 150 pA current pulses respectively. *B.* The response of Vm to a 50 pA hyperpolarizing (Vm held at ~-65 mV; upper traces) and depolarizing (Vm held at ~-100 mV; lower traces) current pulses. Recordings were made in normal ACSF (b1) and then in Ca^{2+} free ACSF (b2), with TTX included in the ACSF. Recording from the same neurone shown in A.

Figure 4 Effect of calcium on the firing pattern of type II interneurone in response to prolonged current injection of a 70 pA depolarising current pulse. **A** shows the firing elicited in the type II interneurone in a slice bathed in normal ACSF, "B" shows the firing when the slice was bathed calcium free ACSF, and "C" the firing when the slice was again bathed in normal ACSF. Note that the burst pattern of firing in "A" is replaced by continuous firing in "B", and that the busrt firing is again seen when the slice is returned to normal ACSF in "C". Traces A1, B1, and C1 show responses of the type II interneurone in A, B, and C respectively at faster scale. D shows the superimposed traces of first spike recorded in A, B and C.

Figure 5. Recordings made from type I neurones.

A recorded type I neurone displays tonic firing to injection of a long duration depolarizing current pulse (upper trace). Midle trace shows the firing frequency and lower trace shows the injected current. *B1.* The recorded type I neurone also displays tonic firing to injection of a 1.5 s depolarising current pulse with the Vm held at around ~-60 mV (horizontal arrows). Upper and middle traces are the neuronal responses to injected current pulses with intensity of Rh and 2*Rh respectively. Lower trace shows superimposed traces of the injected current pulses. *B2.* Recording made when the Vm was hyperpolarized to ~-95mV. Upper and middle traces are the responses to lower and higher intensity of current pulses. Higher current intensity elicits trains of APs with regular intervals. Lower trace shows superimposed traces of injected current pulses. *C1.* Superimposed Vm responses (upper traces) to hyperpolarizing and depolarizing current pulses (lower traces) with addition of TTX in ACSF and with the Vm held at ~-60mV. *C2.* Plot of change in Vm against the intensity of current injection summarized for 4 type I neurones. **The star marks the region of rectification to depolarising current pulses.**

Figure 6. Recordings made from type III neurones.

A. Firing elicited in a type III interneurone by a prolonged depolarising current pulse (upper trace). The interneurone fires briefly near the start of the current injection and

then falls silent, though further brief periods of firing can be elicited by increases in the current injected (vertical arrows). Middle trace shows the firing frequency and lower trace shows the injected current. *B1.* Firing elicited in the same interneurone by a 1.5 s depolarizing current pulse with the Vm held at around ~-60 mV (horizontal arrows). Upper and middle traces are the neuronal responses to injected current pulses with intensity of Rh and 2*Rh respectively. Lower trace is superimposed traces of injected current pulses. *B2.* Recording made when Vm was hyperpolarized to ~-90mV. Upper and middle traces are the response to lower and higher intensity of current pulses. Lower trace is superimposed traces of injected current pulses. *C1.* Superimposed Vm responses (upper traces) to hyperpolarizing and depolarizing current pulses (lower traces) with addition of TTX in ACSF and Vm held at ~-60mV. *C2.* Plot shows change in Vm against the intensity of current injection. **The star marks the region of rectification to depolarising current pulses.**

Figure 7. Measurements of membrane properties.

A. The transmembrane responses (A1, upper traces) to corresponding current injection (lower traces) were averaged from 10 sweeps and the current-voltage relationship was determined; Rn was determined from the slope of the linear portion of the plot **(A2)**. The recording shown was made from a type I neurone. *B.* To measure τ, an averaged transmembrane response to a 0.5 ms hyperpolarizing current **pulse**, usually given at 500 ~ 700 pA, was obtained from at least 1000 sweeps (see insert). The natural logarithm of decay of this potential with time was plotted, with voltage changes occurring within the first 1 ms of the current pulse being ignored. The linear portion of the plot was determined by eye (indicated by arrows), and the best-fit straight line to the intervening data points fitted by method of least square (see dotted lines). The value of τ was then given by the time taken for the voltage to decay to 1/e of its initial value. Data shown here were recorded from a type II neurone. *C.* To measure sag, an averaged transmembrane response was obtained from approximately 20 responses to a 1.5 s hyperpolarizing current pulse, given at 50 pA. The maximum trensmembrane response (ΔV1) and the response before the ending of current injection (ΔV2) were measured. Sag (%) was then obtained using the formula: Sag = $[(\Delta V1 - \Delta V2) \times 100\%]/\Delta V2$. Data shown here were recorded from a type II neurone. *D.* To measure AHP, a single AP was elicited by a 1 ms depolarizing pulse and an averaged response obtained from at least 10 sweeps. Measurements were made to amplitude of fast AHP if this was present (see insert), amplitude of slow AHP, and half decay time of slow AHP, as indicated by arrows and dotted lines. Data shown here were recording made from a type II neurone. *E.* Recordings made from two type-I neurones; it shows that, while the AHP of one neurone was biphasic (upper trace), it was monophasic in the other neurone. All of the

membrane properties were measured with neurones **held** at approximately –55 ~ -60 mV.

Figure 8. Reconstruction of a biocytin filled type-II interneurone.

Figure shows a reconstructed type-II neurone with soma and dendrites drawn in black, and axonal branches in red. The firing characteristic of the neurone is shown insert "a", and location of the interneurone with relation to the trigeminal motor nucleus and other structures is shown in insert "b". Insert "c" shows a photograph of soma and primary dendrites of the neurone, and inserts "d" & "e" show high power photographs of axonal terminals in the Vmot and PCRt-α as indicated by dotted squarea "d" and "e" respectively in the figure. Note the varicosities along the axonal terminals. Small inserts in inserts "d" (lower right panel) and "e" (upper left panel) are phtographs taken using phase contrast optics with foucus on area idicated by dotted circles. Note the contacts of terminals on large soma in "d" (arrow) and small soma in "e". D, dorsal; C, caudal; Vmot, trigeminal motor nucleus; 7n, 7th nerve. **Scale bar=100 μm, 200 μm (b), 20 μm (c), 20 μm (d, e) and 10 μm (small insects in d, e).**

Figure 9. Reconstruction of a biocytin filled type-I interneurone.

Figure shows a reconstructed type-I neurone with soma and dendrites drawn in black, and axonal branches in red. The firing characteristic of the neurone is shown in insert "a", and location of the interneurone and its axonal collaterals, in relation to the trigeminal motor nucleus and other structures, is shown in insert "b". Insert "c", "d" and "e" show high power photographs of axonal terminals in the Vmot (as indicated by dotted square in insert "c"), PCRt-α (indicated by dotted square in "d") and in more caudal areas (indicated by dotted square "e") respectively. Note the contacts of terminals with soma of neurons in the Vmot ("c"; micrograph in lower right panel), PCRt-α ("d"; micrograph in upper right panel), and in more caudal areas ("e"; micrograph in lower right panel), as indicated by arrows in photographs in small inserts. D, dorsal; C, caudal; Vmot, trigeminal motor nucleus; 7n, 7th nerve. **Scale bar=100 μm, 200 μm (b), 20 μm (c), 20 μm (d, e) and 10 μm (small insects in d, e).**

Figure 10. Heterogeneity in axonal projections of type II interneurones.

Reconstructions of three biocytin filled type II interneurones. The soma and dendrites are shown in black and the axon in red. D, dorsal; C, caudal. **Scale bar= 20 μm (a-c), and 100 μm (small insects in a-c)**

Table 1: The passive membrane , spike and AHP properties of trigeminal **Interneurones in the Parvocellular reticular Nucleus (PCRt)**

	Passive Membrane				**Spike**			AHP		
	Vm (mV)	Rn (MΩ)	tau (ms)	Sag (%)	Amp (mV)	H.W. (ms)	Rh (pA)	Fast (mV)	Slow (mV)	H.D. (ms)
Type I	-53.7±0.7 -61~-48 (n=63)	856±71* 198~3517 (n=63)	51.7±2.8 25~76 (n=25)	16.7±2.3 0~55 (n=35)	118±2 81~153 (n=63)	1.8±0.1 0.9~6.6 (n=38)	35±9*** 5~500 (n=63)	9.0±2.1 1.1~27.3 (n=15)	8.9±1.1 2~16.7 (n=20)	104±6 58~161 (n=20)
Type II	-55.1±0.9 -64~-49 (n=48)	625±53 221~1531 (n=48)	55.5±5.7 23~122 (n=19)	16.0±4.2 0~114 (n=35)	113±2 79~140 (n=48)	2.2±0.3 1.1~11.6 (n=48)	74±34 10~1500 (n=48)	7.2±1.8 1.2~19.1 (n=11)	10.9±1.2 3.6~19.6 (n=15)	99±8 59~175 (n=15)
Type III	-55.3±1.4 -62~-50 (n=16)	770±95 234~1690 (n=16)	49.7±4.3 32~74 (n=10)	16.0±2.4 3~29 (n=11)	116±3 80~136 (n=16)	2.1±0.2 1.2~3.7 (n=10)	28±6 10~120 (n=16)	2.9±1.8 1.1~4.6 (n=2)	6.3±1.7* 1.9~11.4 (n=6)	69±13 21~108 (n=6)

Data given are mean±standard error, range and sample size.

Significance: *p<0.05, ***p<0.005 compared to type II

Table 2: Geometric Data for Trigeminal **Interneurones in the PCRt**

	Soma			***Dendrites***		
	Major diameter (μm)	Minor diameter (μm)	Somata surface ($\times 10^3 \mu m^2$)	Dendrites per neurone	End-terminals per dendrites	Dendritic length (μm)
Type I	**17.1±0.5***	**11.1±0.3**	**0.16±0.01**	**3.9±0.2**	**3.8±0.3**	**142±5**
	12 ~ 28	**7~15**	**0.75~0.24**	**2~7**	**1~26**	**9~481**
	n=35	**n=35**	**n=35**	**n=35**	**n=137**	**n=503**
	(17.9±0.6)	(11.1±0.5)	(0.16±0.01)	(4.07±0.4)	(3.5±0.4)	(155±7)
	(15~25)	(7~14)	(0.10~0.23)	(2~7)	(1~13)	(13~481)
	(n=15)	(n=15)	(n=15)	(n=15)	(n=61)	(n=214)
Type II	**20.1±1.1**	**11.5±0.5**	**0.18±0.01**	**3.8±0.2**	**3.4±0.4**	**143±6**
	13 ~ 40	**7~17**	**0.82~0.32**	**2~6**	**1~16**	**55~495**
	n=21	**n=21**	**n=21**	**n=21**	**n=79**	**n=268**
	(21.9±2.5)	(11.2±0.5)	(0.19±0.02)	(4.33±0.4)	(3.4±0.6)	(136±8)
	(15~40)	(10~14)	(0.12~0.31)	(3~6)	(1~16)	(5~378)
	(n=9)	(n=9)	(n=9)	(n=9)	(n=39)	(n=151)
Type III	**15.7±1.4**	**11.3±0.6**	**0.14±0.01**	**4±0.5**	**4.33±0.7**	**119±8**
	12~21	**10~14**	**0.10~0.17**	**3~6**	**1~15**	**11~364**
	n=6	**n=6**	**n=6**	**n=6**	**n=24**	**n=104**
	18	11	0.16	6	2.5±0.96	88.4±14
	(n=1)	(n=1)	(n=1)	(n=1)	1~7	27~191
					(n=6)	(n=15)

Data given are mean±standard error, range and sample size.

Data in **parentheses** are from neurons whose axonal arborisation are clearly seen in Vmot

Significance: * $p<0.05$, compared to Type II

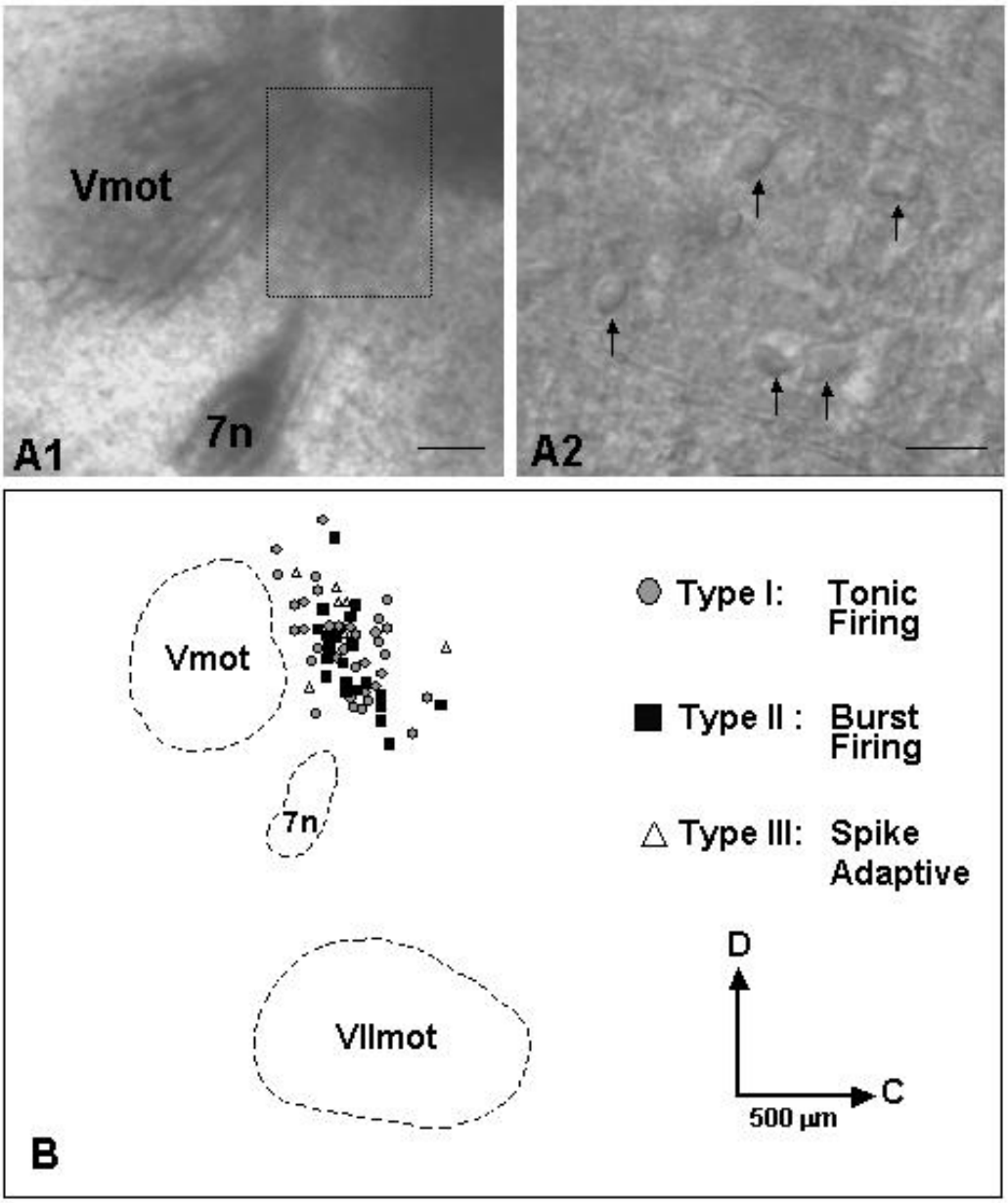

Fig. 1, Min et al, EJN-2003-05-05791

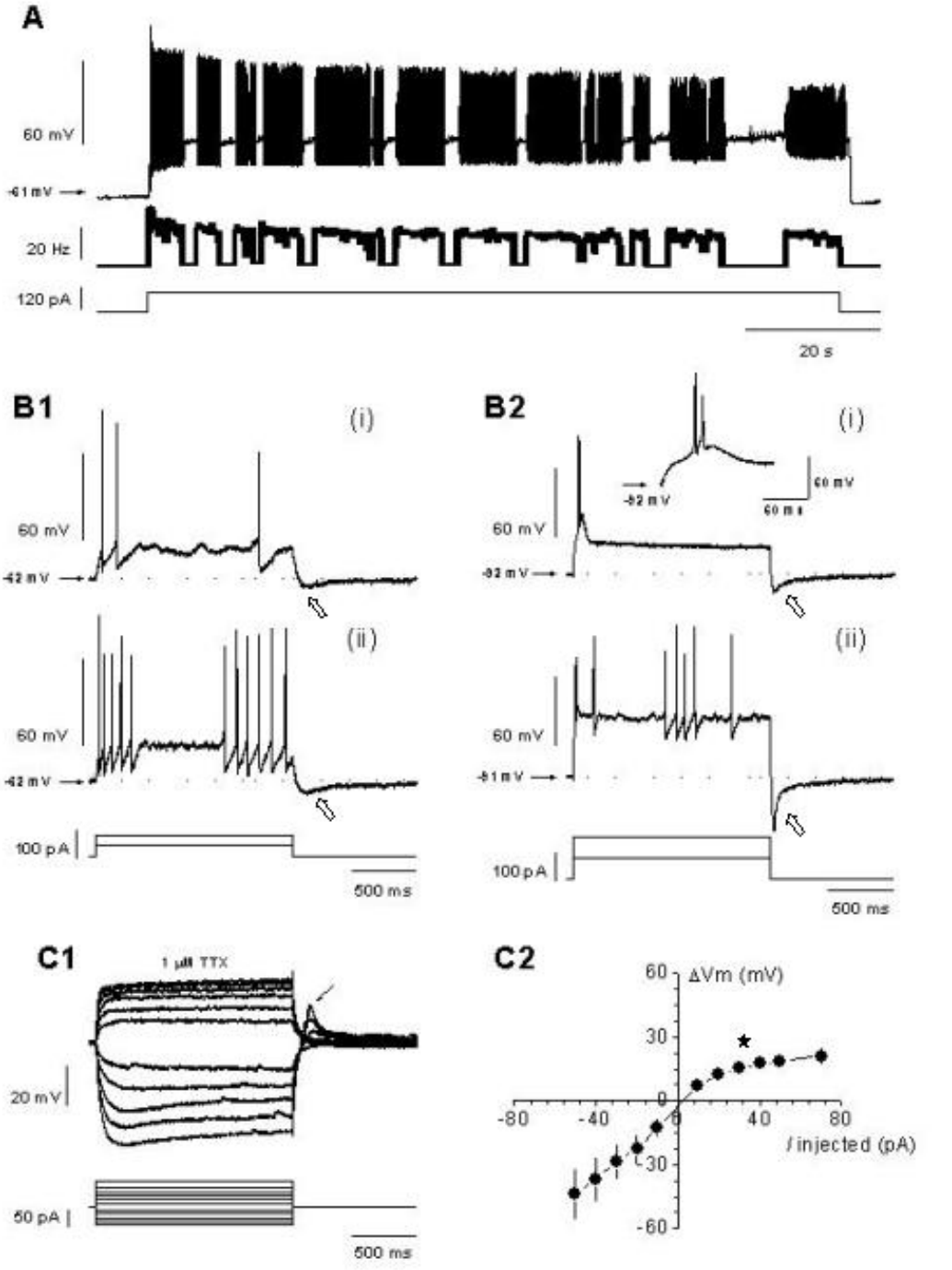

Fig. 2, Min et al, EJN-2003-05-05791

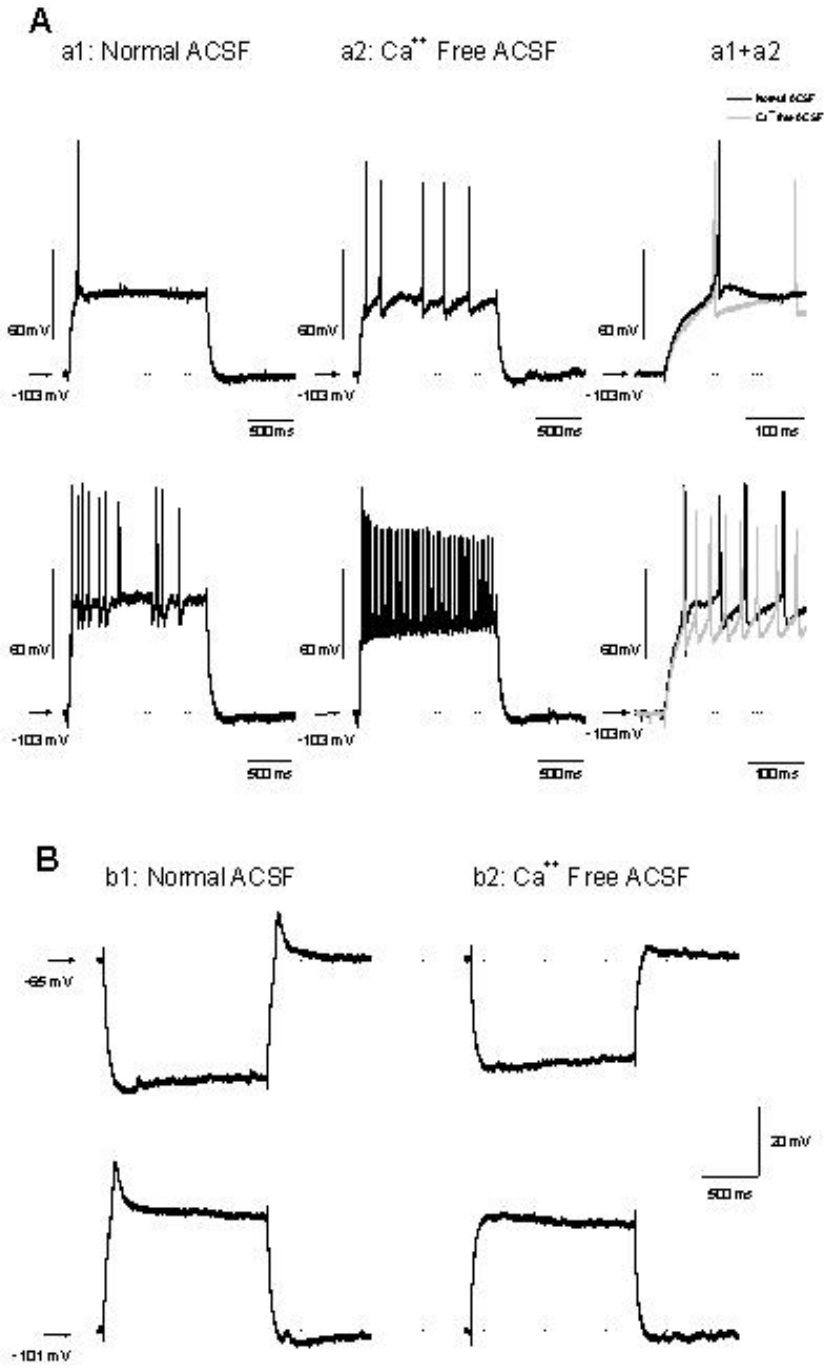

Fig. 3, Min et al, EJN-2003-05-05791

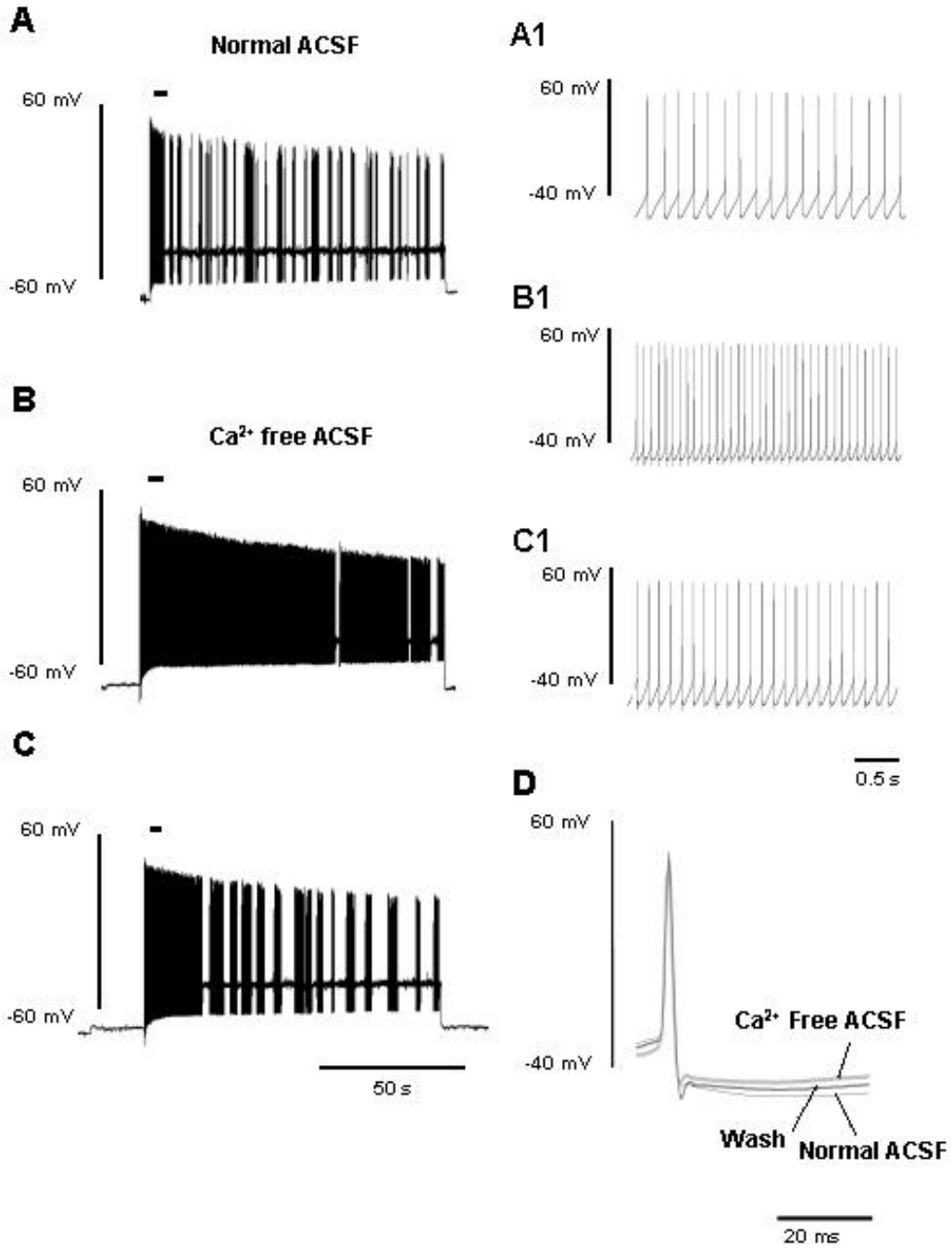

Fig. 4, Min et al, EJN-2003-05-05791

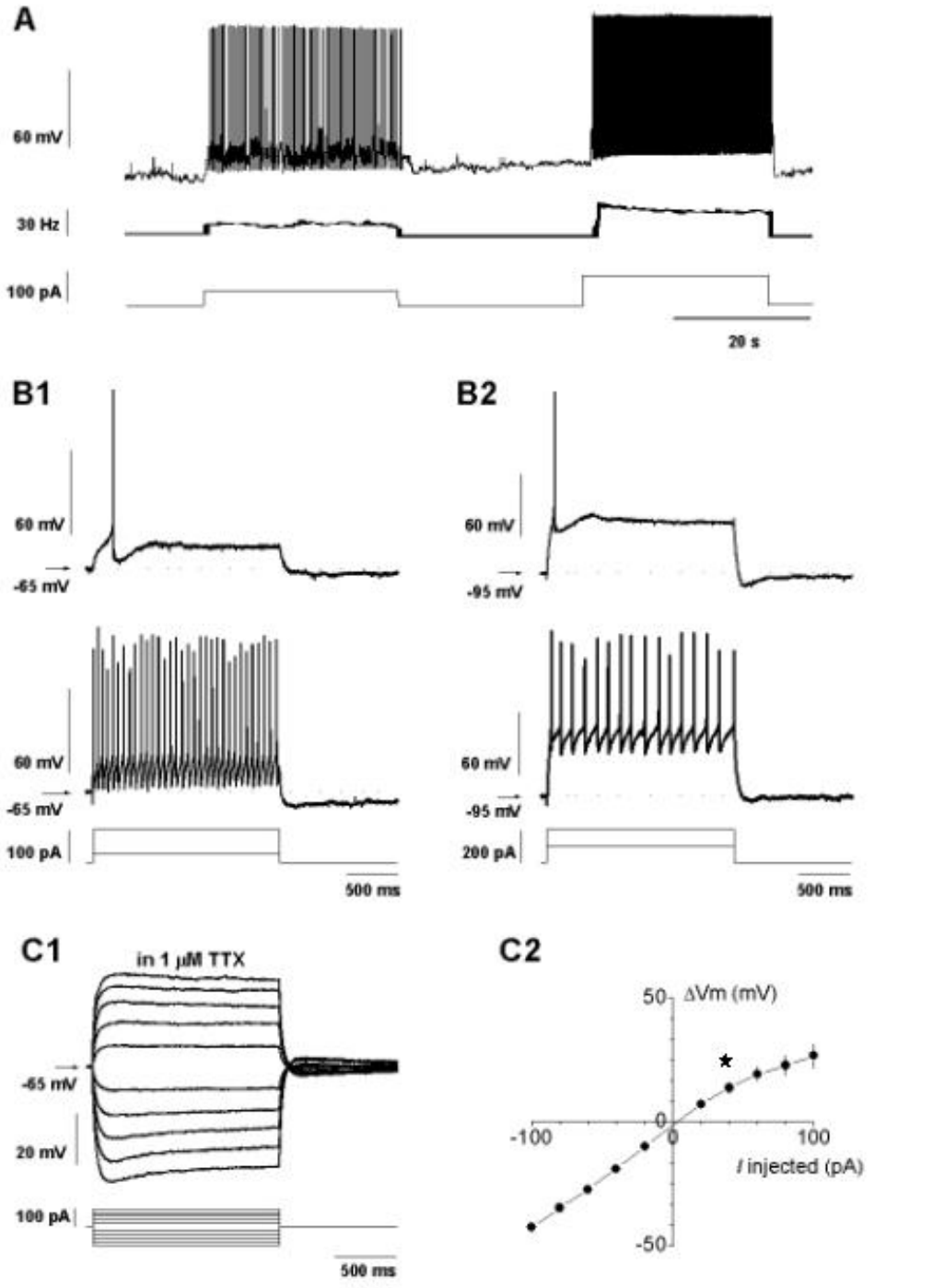

Fig. 5, Min et al, EJN-2003-05-05791

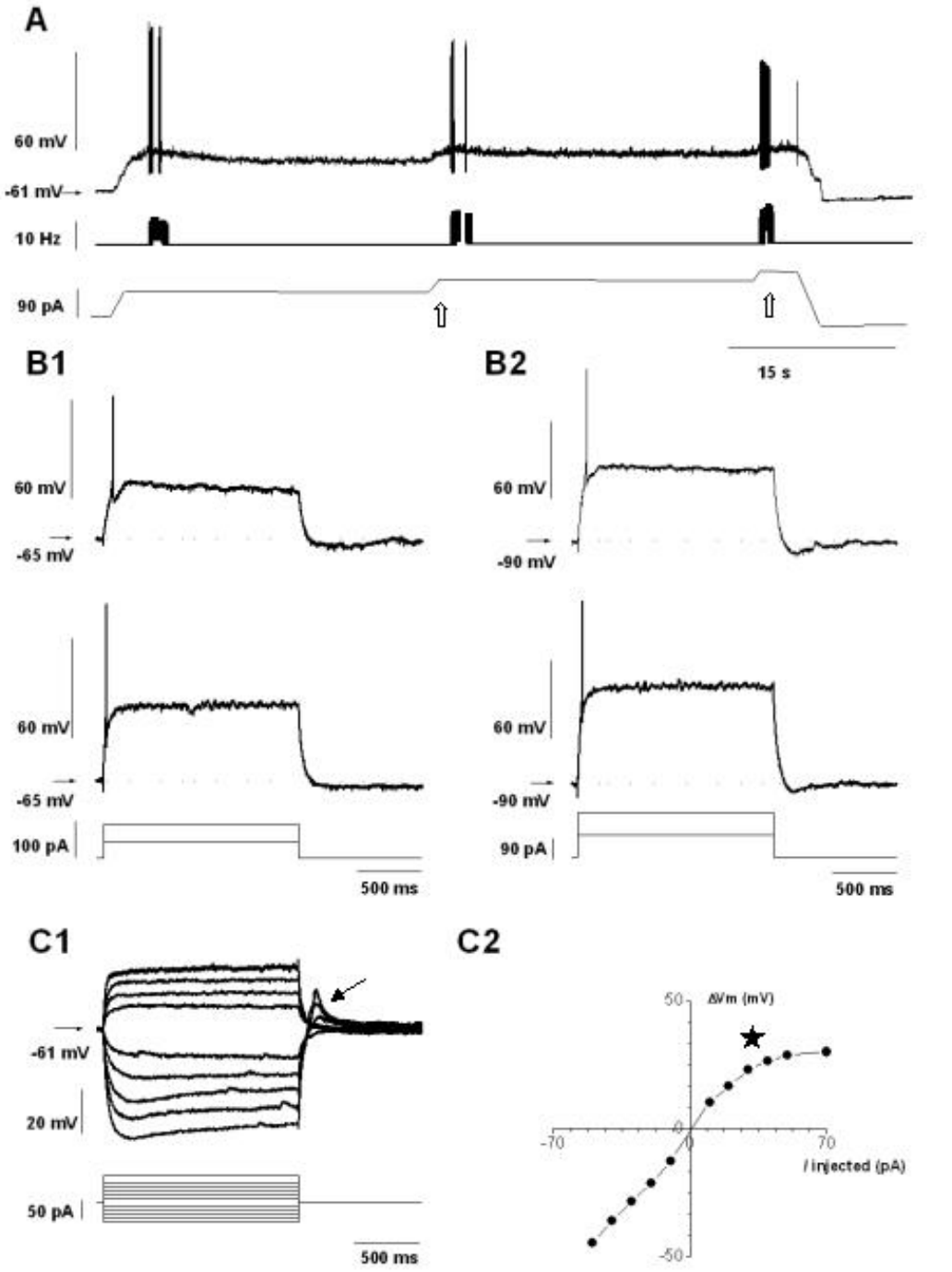

Fig. 6, Min et al, EJN-2003-05-05791

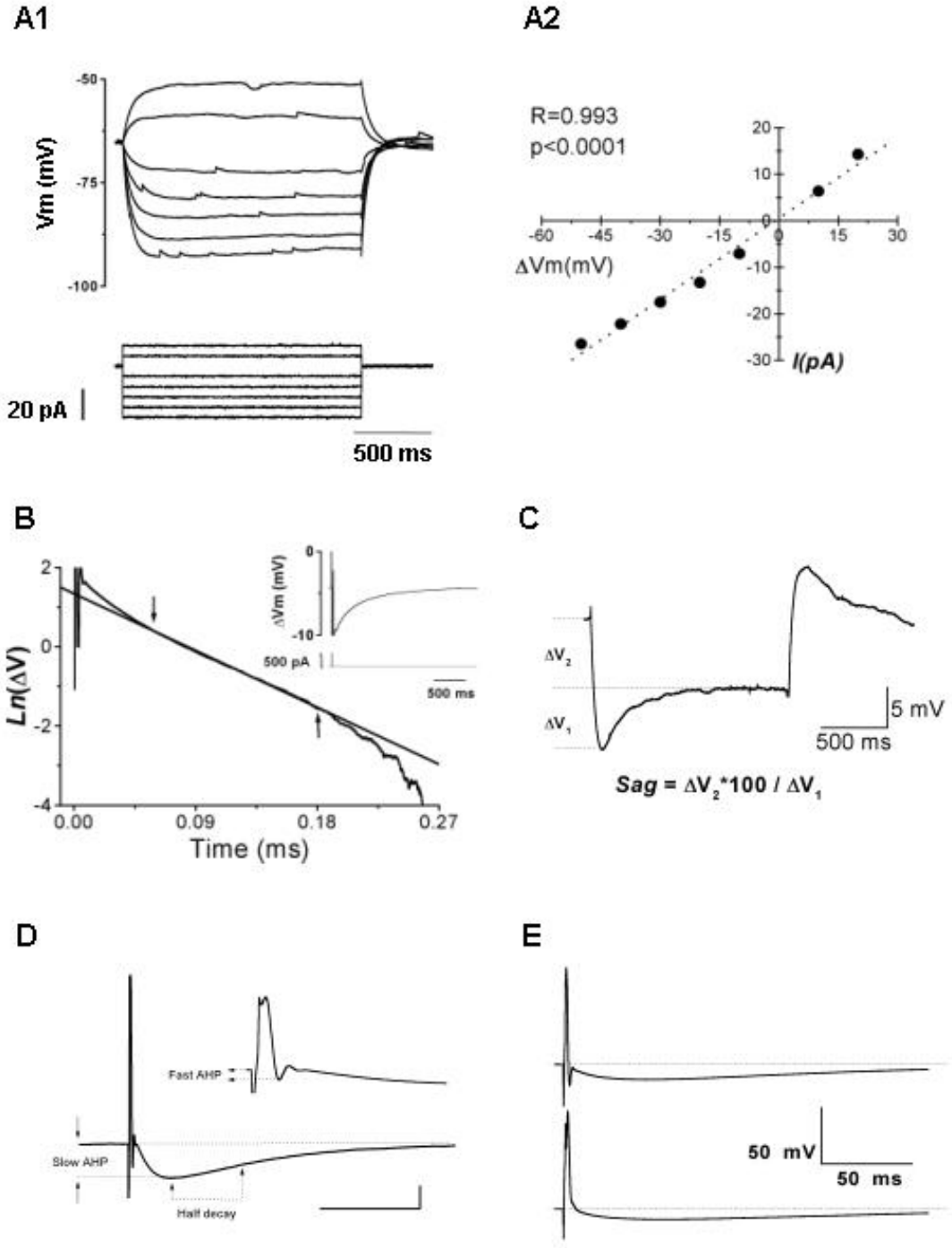

Fig. 7, Min et al, EJN-2003-05-05791

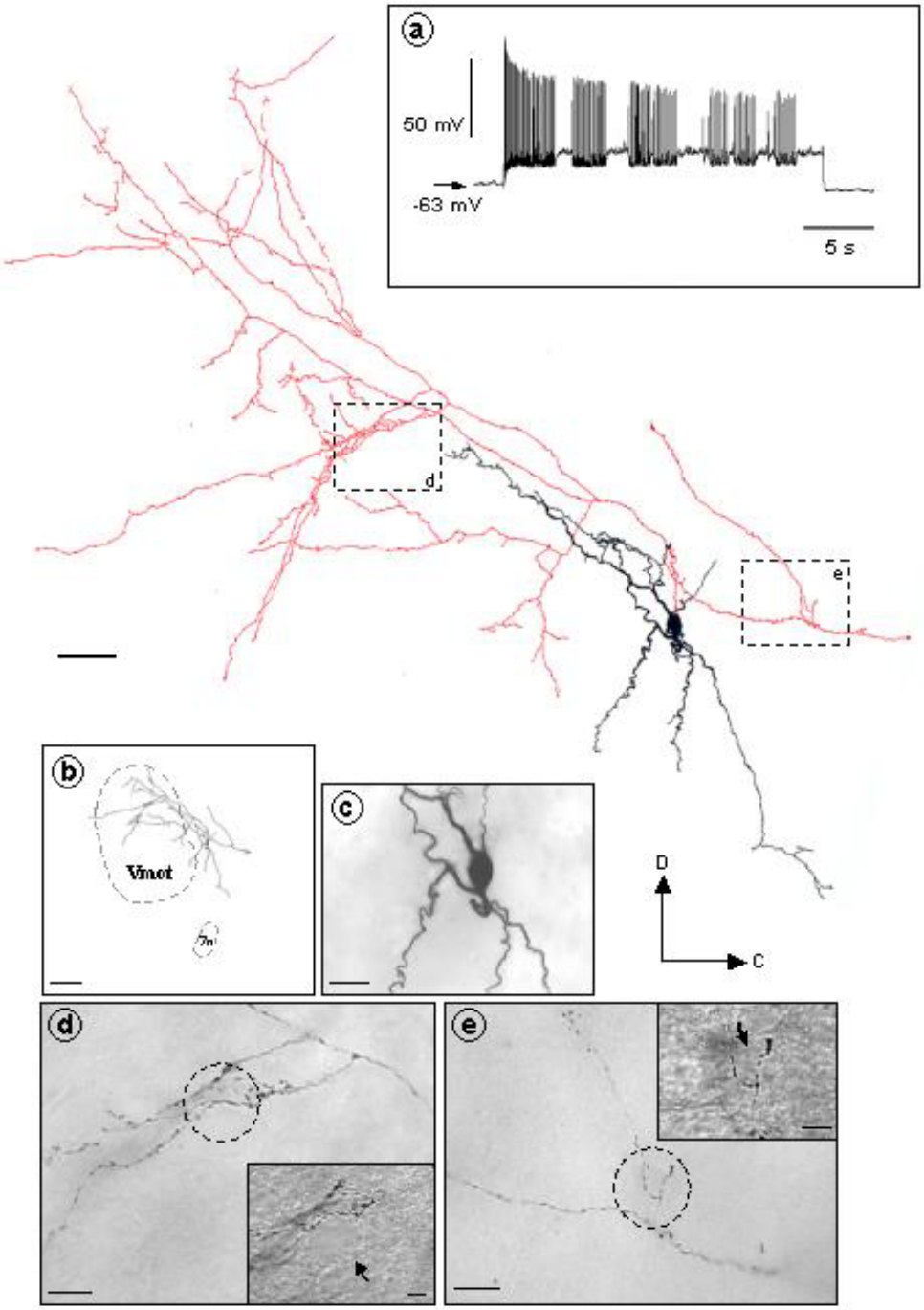

Fig. 8, Min et al, EJN-2003-05-05791

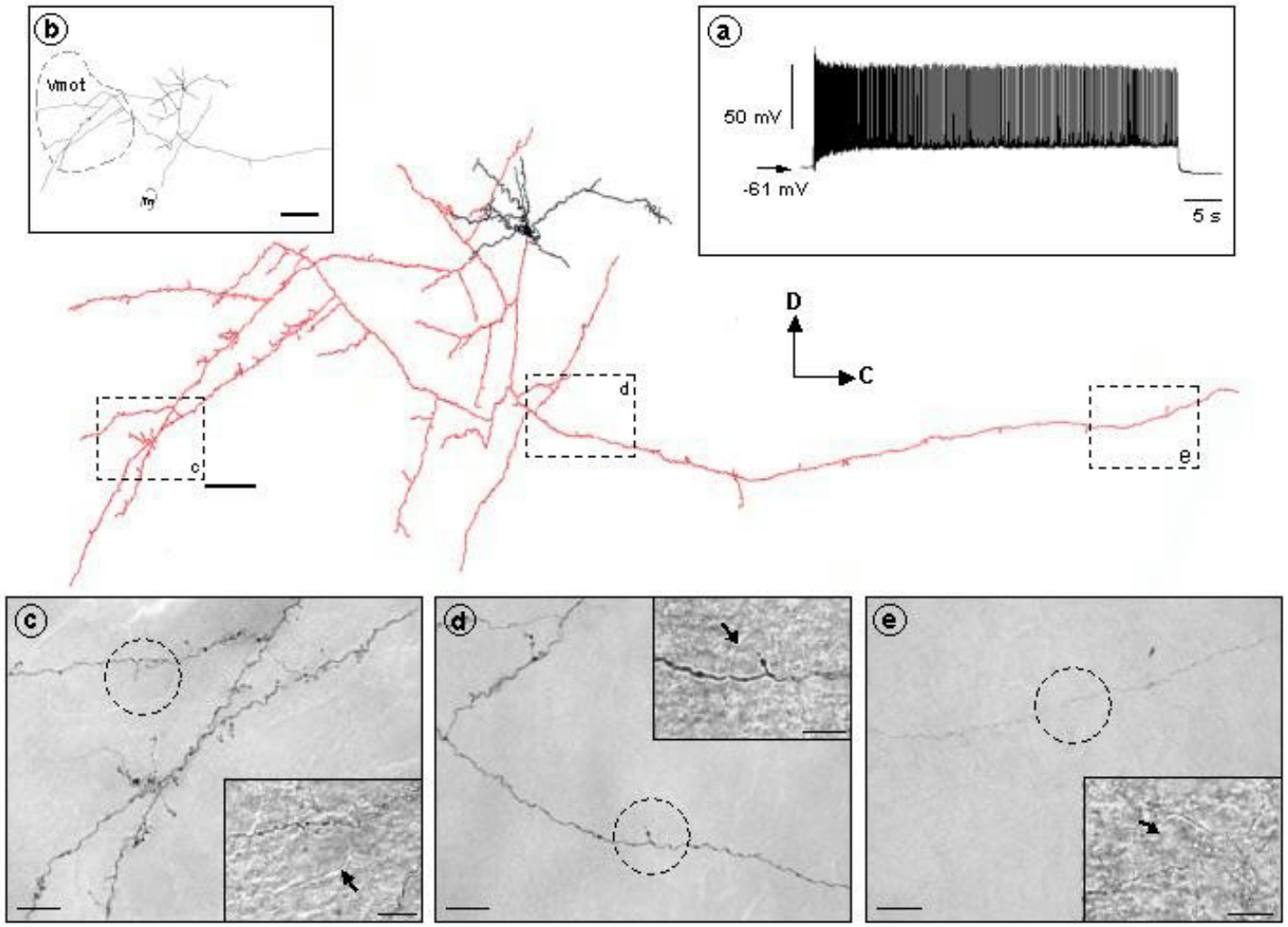

Fig. 9, Min et al, EJN-2003-05-05791

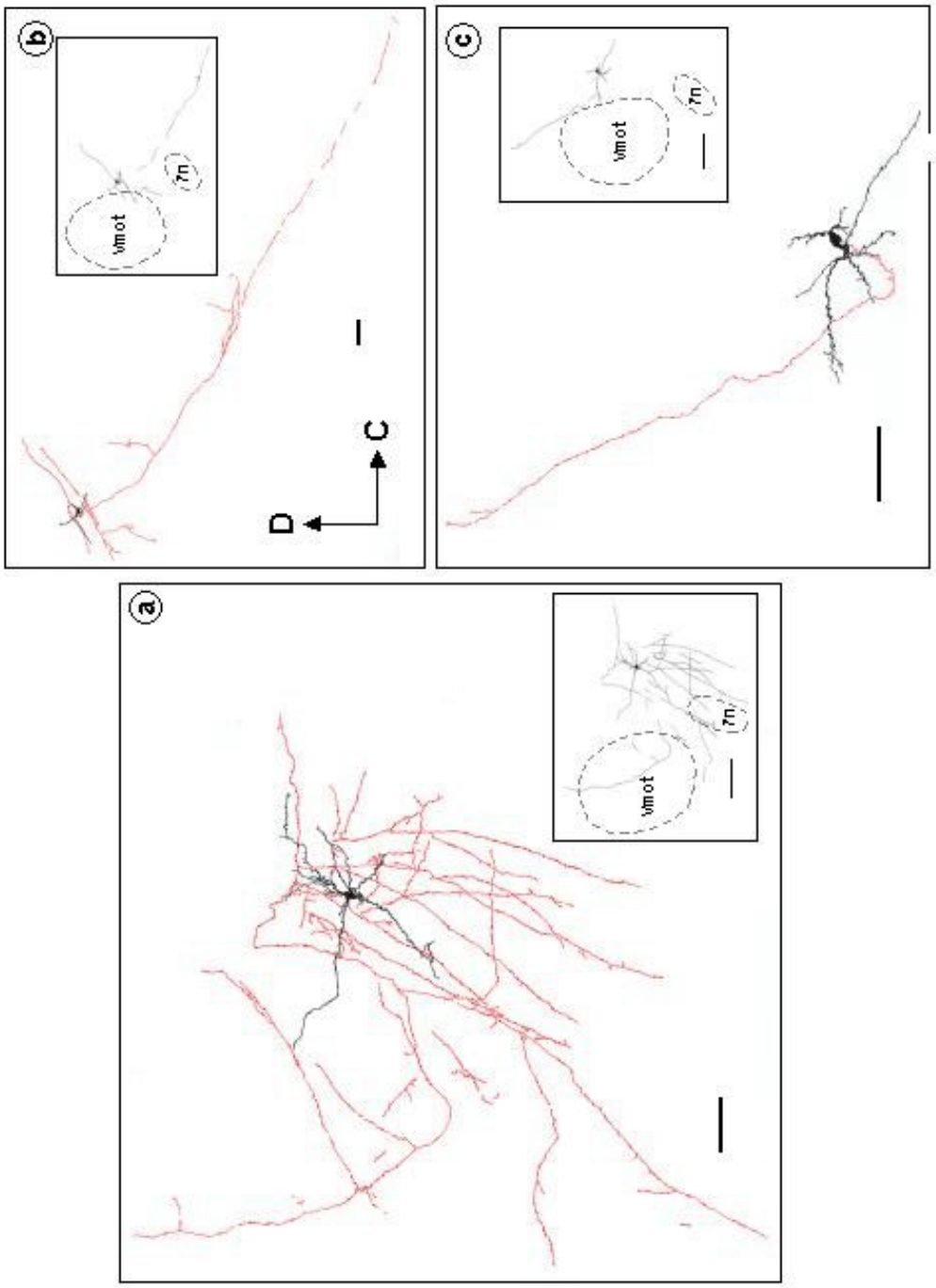

Fig. 10, Min et al, EJN-2003-05-05791